Vibrational Symmetry Breaking of NO_3^- in Aqueous Solution: NO Asymmetric Stretch Frequency Distribution and Mean Splitting†

ARTICLE *in* THE JOURNAL OF PHYSICAL CHEMISTRY A · AUGUST 2009

Impact Factor: 2.69 · DOI: 10.1021/jp903626t

Vibrational Symmetry Breaking of NO_3^- in Aqueous Solution: NO Asymmetric Stretch Frequency Distribution and Mean Splitting†

Sai G. Ramesh,§ Suyong Re,§,¶ Jean Boisson,§ and James T. Hynes*,§,‡

Chemistry Department, École Normale Supérieure, and Centre National de la Recherche Scientifique, Unité Mixte de Recherche 8640, 24 rue Lhomond, 75005 Paris, France, and Department of Chemistry and Biochemistry, University of Colorado, Boulder, Colorado 80309-0215

Received: April 20, 2009; Revised Manuscript Received: July 13, 2009

We apply a solute−solvent approach to a theoretical study of vibrational symmetry breaking in aqueous NO_3^- solution. Experimental infrared and Raman spectra have shown that the NO asymmetric stretches, which are degenerate for the isolated anion, are split by 35−60 cm^{-1} in dilute solution. As an initial step to calculating the spectra, we have computed the distribution of energies, or the "static spectrum", and the resulting mean splitting of the two NO asymmetric stretch eigenstates in an aqueous milieu. These have been obtained in a two-mode treatment that considers only the NO asymmetric stretch mode pair as well as a full six-mode treatment. In both sets of calculations, six eigenstates, namely, the ground state, the two NO asymmetric stretch fundamentals, and its three overtones, were determined to suffice for converged energy distributions and mean splittings. The couplings between these six states are driven by the solvent forces on the anion's modes, which were extracted from molecular dynamics simulations. The solvent forces on the two central modes were found to give rise to a majority of the computed mean splitting of 21.7 cm^{-1}. The distribution of NO asymmmetric stretch excitation energies with these two modes alone was found to have a Maxwell−Boltzmann shape. The solvent forces on the in-plane bends were found to modestly reduce the splitting size and slightly alter the width of the parent distribution. The symmetric stretch force was found to have no effect on the splitting but instead resulted in a widening on the distribution shape. The force gradients were found to have a weak effect on both the eigenvalue distribution and the mean splitting.

1. Introduction

The nitrate anion, NO_3^-, is a key species in the atmospheric sciences. Its mineral salts are very hygroscopic, so that aerosols containing them are able to seed cloud formation.[1] Important heterogeneous chemistry, including stratospheric ozone depletion,[2] occurs on nitrate aerosols. NO_3^- is relevant in various other atmospheric contexts,[3−5] often in connection with the issue of its production via acid dissociation of nitric acid HNO_3 at aqueous aerosol surfaces, a topic of much recent experimental[7] and theoretical[6] research; for an extensive discussion, see ref 6a.

The anion is also important in its own right in the solution chemistry context. NO_3^- can function as a probe of its local environment via, say, the spectroscopy of its six vibrational modes. Conversely, the solvent effect on the intramolecular dynamics has attracted considerable interest. For example, Waterland et al. have considered the photodynamics of the NO_3^- in hydrogen bonding and polar solvents using resonance Raman spectroscopy.[8] In connection with the anion as a probe, many infrared (IR) and Raman spectral investigations were published in the late 1960s and early 1970s for several nitrate salts and a range of concentrations, tending toward the high end.[9] These works drew inferences on the nature of the anion hydration and specific cation effects based upon the changes in the positions and widths of NO_3^-'s vibrational bands. More recent results along these lines are due to Zhang et al.,[10] Grassian and coworkers,[1] and Liu et al.[11]

Of the vibrational bands observed in the above studies, the NO asymmetric stretch band (ν_3, ∼1370 cm^{-1}) features prominently. It is the most intense infrared band. The underlying pair of NO asymmetric stretch vibrations is degenerate for the D_{3h}-symmetric isolated anion. The absence of spatial symmetry in solution lifts the degeneracy of the NO asymmetric stretches, resulting in a doublet in both IR and Raman spectra. This effect has been referred to as "symmetry breaking" and is the focus of this article.[12] While this band splitting increasing with concentration, a splitting of 35−60 cm^{-1} has been reported in dilute solutions.[1,8−11] On this basis, it has been suggested that the symmetry breaking can arise from the nitrate−water interaction alone; it does not require a cation's presence, though the effect is clearly enhanced by it. Keeping to this dilute limit, this article presents an initial theoretical study on the ν_3 symmetry breaking in aqueous NO_3^-.

Theoretical studies of nitrate symmetry breaking are few in number, including ab initio computations on nitrate−water clusters[1,8,11] as well as mixed quantum NO_3^-−classical H_2O (QM/MM) simulations.[13] The former have been typically coupled with experimental work. Among them, Waterland et al. have combined ab initio data with neutron scattering and Raman spectral data on several crystalline nitrates to relate the root-mean-square NO bond length distortion to the NO asymmetric stretch frequency splitting.[8] QM/MM simulations by Lebrero et al. showed periods of time, lasting about 100−200 fs, where a NO bond length and its oxygen's negative charge are both larger or smaller than those for the other two NO bonds.[13] More

† Part of the "W. Carl Lineberger Festschrift".

* To whom correspondence should be addressed. E-mail: hynes@spot.colorado.edu.

§ École Normale Supérieure, and Centre National de la Recherche Scientifique.

‡ University of Colorado.

¶ Present address: Theoretical Biochemistry Laboratory, RIKEN Advanced Science Institute 2-1, Hirosawa, Wako, Saitama 351-0198, Japan.

10.1021/jp903626t
Published on Web 08/18/2009

TABLE 1: Vibrational Modes and Harmonic Frequencies (in cm^{-1}) of D_{3h}-Symmetric NO_3^-

label	mode	symm.	ω_i^a
1	NO sym. stretch	A_1'	1056.7
2	out-of-plane (OOP) bend	A_2''	830.8
(3x, 3y)	NO asym. stretch	E′	1407.0
(4x, 4y)	ONO in-plane bends	E′	734.0

[a] The ω_i have been adjusted for a better match with available aqueous-phase fundamental energies. See Appendix A.2.

recently, Boisson et al. have shown through QM/MM simulations that two interleaved sets of such bond length asymmetric structures can be defined.[14,15] One set is only slightly more populated than the other, and the anion switches between them with a fast, 100 fs time scale. However, these valuable previous efforts have not provided a theoretical framework for the interpretation of the spectrum and the splitting; we take a first step in that provision here.

The present work, as part of our ongoing studies on nitrate hydration,[14−16] attempts a more complete quantum treatment of NO_3^-'s vibrations, and thereby the symmetry breaking, by employing the perturbative solute−solvent coupling method. We focus upon the manner in which water solvent forces on the anion, derived from molecular dynamics simulations, influence the distribution of excitation energies and the resulting mean splitting of the NO asymmetry stretch (ν_3) band. The question of whether the forces on the two central NO asymmetric stretch modes alone suffice to explain the observed effect is addressed. Further, the effects of including the solvent forces on the remaining four modes are also analyzed. We shall be primarily concerned with average measures in this article, postponing to the future a study of the dynamics in the system, including the aqueous-phase infrared spectrum of NO_3^-, and the origin of the solvent forces on its vibrations.

The remainder of this article is organized as follows. We start in section 2 with definitions of a few essential quantities and outline the scheme of our calculations using them. A simplification of the symmetry breaking problem to the two core NO asymmetric stretch modes is attempted in section 3, where we compare classical and quantum treatments. Section 4 describes a progressive advance from the two-mode to the full, six-mode treatment of the problem. We summarize our findings and conclude in section 5.

2. Preliminaries

Table 1 shows the vibrational modes of nitrate, numbered as per spectroscopic convention. The x, y tags for the doubly degenerate E′ modes come from the axis along which the N atom motion points. The relative atomic displacements for our target modes, the NO asymmetric stretches, are depicted in Figure 1.

The Hamiltonian for the reference D_{3h}-symmetric anion is written as

$$H_o = \sum_i \frac{1}{2}\omega_i(P_i^2 + Q_i^2) + V_{anh}(\mathbf{Q}) \qquad (1)$$

This form implies that we use a single reference NO_3^- structure to treat symmetry breaking, as opposed to (multiple) in-plane distorted ones. Since it is not immediately obvious that our choice suffices, we give our reasoning in Appendix A.1. As the harmonic part of H_o shows, the $\mathbf{Q}$ are rectilinear normal coordinates in unitless form. The harmonic frequencies, ω_i, that we use in this article have been adjusted to better suit the mean

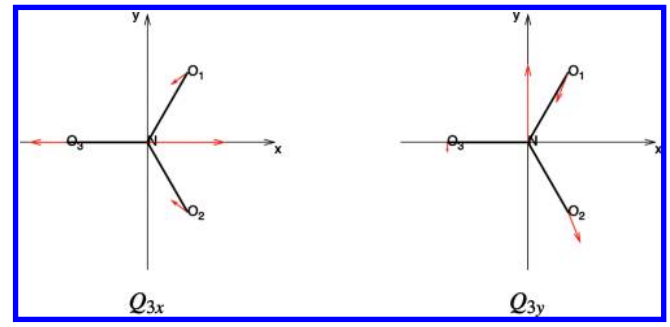

Figure 1. The degenerate NO asymmetric stretch normal modes.

vibrational data in the aqueous milieu; these numbers are shown in Table 1. The anharmonic vibrational potential is developed as a Taylor series to sixth order. The details of the computation of the ω_i and V_{anh} are presented in Appendix A.2.

The solvent influence on these vibrations is contained in the interaction potential

$$\delta V(t) = -\sum_i F_i Q_i - \sum_{i\le j} G_{ij} Q_i Q_j \qquad (2)$$

As its notation signifies, $\delta V(t)$ is the fluctuating part of the solute−solvent interaction, $\langle \delta V(t)\rangle = \langle F_i\rangle = \langle G_{ij}\rangle = 0$. The average, constant part that we have subtracted usually provides the gas-to-solution-phase frequency shifts.[17] We have effectively absorbed it into H_o by the adjustment of the ω_i. The time evolution of the forces (F_i) and force gradients (G_{ij}) on the NO_3^-'s modes, which are evaluated at the equilibrium geometry of the anion, is governed by the solvent dynamics. For the present calculations, we carry out molecular dynamics simulations with the NO_3^-−H_2O force field developed by Thomas et al.;[18] Appendix B gives the specifics of the simulations. An important result is that the simulation forces and force gradients have Gaussian distributions, with $\sigma(F_i) \approx 100$ cm^{-1} ($\sim$180 cm^{-1} for F_2) and $\sigma(G_{ij}) \approx 1-10$ cm^{-1}.

We analyze symmetry breaking in aqueous nitrate through the solution of

$$H(t) = H_o + \delta V(t) \qquad (3)$$

Its quantum treatment, the solute−solvent coupling approach, shall occupy most of this article, and it involves the following scheme. H_o is cast as a matrix in a basis of multimode harmonic product functions. Diagonalization of this matrix gives the eigenstates ψ_i, and eigenvalues $E_{o,i}$. These are then used to construct matrix elements for eq 3

$$\begin{aligned} H_{ij}(t) &= E_{o,i}\delta_{ij} + \delta V_{ij}(t) \\ \delta V_{ij}(t) &= \langle \psi_i|\delta V(t)|\psi_j\rangle \end{aligned} \qquad (4)$$

We identify the eigenfunctions with sizable NO asymmetric stretch character in the solution of $H(t)$. The description of these eigenfunctions and their eigenvalues are the pieces of information that we shall need in this partial study of the symmetry breaking in aqueous NO_3^-. The quantum treatment will be interspersed with a simpler, classical approach as needed.

The role of the solvent forces, F_i, in the title phenomenon is the primary focus of this article. We eschew a cumbersome notational distinction between forms of $\delta V(t)$ with and without

the force gradients, G_{ij}. Unless explicitly indicated otherwise, $\delta V(t)$ henceforth means only the linear part of eq 2.

3. Two-Mode Analysis

Instead of directly plunging into a full six-mode treatment of symmetry breaking, we first examine only the two NO asymmetric stretches, Q_{3x} and Q_{3y}. This two-mode simplification is of intrinsic value as it is apt to be transparent, and its results can serve as a reference for the more complex six-mode problem. For this section alone, the 3 in the mode subscripts is dropped.

The Hamiltonian for this two-mode (2m) subproblem is

$$\begin{aligned} H^{2m}(t) &= H_o^{2m} + \delta V^{2m}(t) \\ H_o^{2m} &= \frac{1}{2}\omega(P_x^2 + P_y^2) + \frac{1}{2}\omega(Q_x^2 + Q_y^2) + f(Q_x^3 - 3Q_xQ_y^2) \\ \delta V^{2m}(t) &= -F_xQ_x - F_yQ_y \end{aligned} \tag{5}$$

where we have retained only the cubic anharmonicity. Its particular form reflects the three-fold symmetry of the anion. The anharmonicity constant, f, is a negative number, and our ab initio computations, described in Appendix A.2, yield a value of $-49.4\ cm^{-1}$. $\delta V(t)$ has been limited to just the solvent forces, assuming their dominance in the solvent influence; these will be checked by including the force gradients at the end of the analyses.

3.1. Classical Treatment. With only a few terms present, $H^{2m}(t)$ lends itself to a simple classical treatment. The starting point is the observation that $Q_x = Q_y = 0$ is not the equilibrium position for the two-mode potential. A completion-of-squares step

$$\frac{1}{2}\omega(Q_x^2 + Q_y^2) - F_xQ_x - F_yQ_y = \frac{1}{2}\omega\left[Q_x - \frac{F_x}{\omega}\right]^2 + \frac{1}{2}\omega\left[Q_y - \frac{F_y}{\omega}\right]^2 - \frac{F_x^2 + F_y^2}{2\omega}$$

eliminates the linear terms and yields $(F_x/\omega, F_y/\omega)$ as the instantaneous potential minimum. The above equation signals for a change of variables

$$\begin{aligned} Q_x' &= Q_x - \frac{F_x}{\omega} \qquad P_x' = P_x \\ Q_y' &= Q_y - \frac{F_y}{\omega} \qquad P_y' = P_y \end{aligned}$$

Upon re-expressing the cubic anharmonicity in the new variables, additional quadratic terms are generated. The new Hamiltonian now reads

$$H^{2m}(t) = \frac{1}{2}\omega(P_x'^2 + P_y'^2) + \frac{1}{2}[Q_x'\ Q_y'] \times \begin{bmatrix} \omega - 2\alpha F_x & 2\alpha F_y \\ 2\alpha F_y & \omega + 2\alpha F_x \end{bmatrix} \begin{bmatrix} Q_x' \\ Q_y' \end{bmatrix} + f(Q_x'^3 - 3Q_x'Q_y'^2) + \ldots \tag{6}$$

where the coefficient gauging the nitrate−solvent coupling is

$$\alpha = -\frac{3f}{\omega} \tag{7}$$

This coefficient will be important throughout this paper. With the values of f and ω quoted above, $\alpha \approx 0.1$. The ellipsis in eq 6 represents dropped constant and linear terms. The prefactors for the latter contain α^n, $n \geq 2$, that lead to weak secondary effects.

Our focus is the modified quadratic portion of eq 6, from which we wish to extract new frequencies. To this end, we define the polar form of the forces

$$F = \sqrt{F_x^2 + F_y^2} \qquad \theta(t) = \tan^{-1}(F_y/F_x)$$
$$\mathbf{R}(t) = \begin{bmatrix} \cos\frac{1}{2}\theta & \sin\frac{1}{2}\theta \\ -\sin\frac{1}{2}\theta & \cos\frac{1}{2}\theta \end{bmatrix} \tag{8}$$

Applying a coordinate rotation $\mathbf{Q}' = \mathbf{R}(t)\mathbf{Q}''$, the 2×2 matrix of force constants is transformed as

$$\mathbf{R}(t)^T \begin{bmatrix} \omega - 2\alpha F_x & 2\alpha F_y \\ 2\alpha F_y & \omega + 2\alpha F_x \end{bmatrix} \mathbf{R}(t) = \begin{bmatrix} \omega - 2\alpha F & 0 \\ 0 & \omega + 2\alpha F \end{bmatrix} \tag{9}$$

The quadratic part of two-mode Hamiltonian simplifies to

$$\frac{1}{2}[\omega P_x''^2 + (\omega - 2\alpha F)Q_x''^2] + \frac{1}{2}[\omega P_y''^2 + (\omega + 2\alpha F)Q_y''^2]$$

for which

$$\omega'' = \sqrt{\omega(\omega \pm 2\alpha F)} \approx \omega \pm \alpha F \tag{10}$$

are the new frequencies.

The two variable changes above express the modification of the character of the degenerate pair of NO asymmetric modes due to the solvent. It is particularly clear that F_x and F_y have no effect without the intramolecular anharmonicity. The most conspicuous change is, of course, that the harmonic

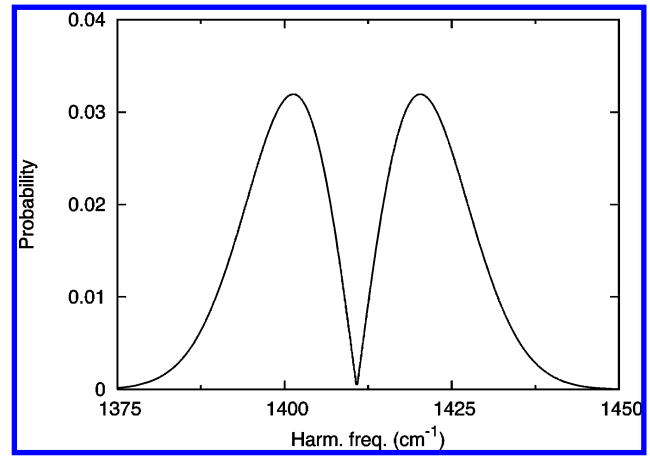

Figure 2. Distribution of split harmonic frequencies of the NO asymmetric stretches based on the distribution of the solvent force magnitude, $\rho(F)$, on them. See text around eq 11.

frequencies of the new modes are split by $2\alpha F$ ($= -6fF/\omega$). To leading order, this is the extent of symmetry breaking within the two-mode framework.

For any given distribution of F_x and F_y, $\langle F \rangle > 0$, resulting in some nonzero mean splitting of harmonic frequencies. The simulations described in Appendix B yield F_x and F_y as uncorrelated quantities, both with a Gaussian spread of the same width σ. The distribution for F is therefore the product of these Gaussians with the angle integrated out, $\rho(F) = F/\sigma^2 \exp(-F^2/2\sigma^2)$. With this, and the estimates $\alpha \approx 0.1$ and $\sigma(F) \approx 95$ cm^{-1}, we depict the distribution of the split frequencies $\omega \pm \alpha F$ in Figure 2. The mean splitting for this distribution will be

$$2\alpha\langle F \rangle = \sqrt{2\pi}\alpha\sigma \tag{11}$$

whose numerical value is 23.8 cm^{-1}. This compares reasonably well to the 35 cm^{-1} experimental estimate by Hudson et al.; see Figure 3 of ref 1b.

We now introduce the force gradients from eq 2

$$-G_{xx}Q_x^2 - G_{xy}Q_xQ_y - G_{yy}Q_y^2$$

into $\delta V^{2m}(t)$. Clearly, these directly affect the quadratic potential. Working through the coordinate transformations, we obtain the modified frequencies as

$$\omega'' \approx \omega \pm \frac{1}{2}\sqrt{[2\alpha F_x + (G_{xx} - G_{yy})]^2 + [2\alpha F_y - G_{xy}]^2} \tag{12}$$

This equation and eq 10 are the two-mode analogues of the solvent-induced frequency change formula for a single oscillator that has been severally employed in the literature.[19]

To estimate the size of the splitting with the force gradients, we employ the simulation results (Appendix B) that the G_{ij}'s also have a Gaussian distribution. The ones we need have the widths $\sigma(G_{xx} - G_{yy}) = \sigma(G_{xy}) \approx 3.3$ cm^{-1}. Taking four terms under the square root in eq 12 to have mutually uncorrelated Gaussian distributions, we randomly sample values for them. This procedure yields a splitting of 24.1 cm^{-1}, a value which hardly differs from the estimate with F_x and F_y alone.[20]

3.2. Two-Mode Quantum Treatment: Identification of a Core-State Sextet. Turning now to a quantum analysis, our first task is to obtain eigenstates and eigenvalues of H_o^{2m} in eq 5. We choose a rather small basis, consisting of only the harmonic product functions with a total of 0, 1, and 2 quanta of vibrational excitation in the NO asymmetric stretch modes, Q_x and Q_y. This makes for a basis size of 6, and we shall demonstrate its sufficiency a few lines below. The notation $3_m^x 3_n^y$ refers to a product basis function with m and n vibrational quanta in Q_x and Q_y, respectively. (The 3 comes, of course, from the spectroscopic numbering scheme in Table 1.)

When symmetrized, the basis is partitioned into three pairs, namely, A_1': 0_0 and $[1/2^{1/2}](3_2^x + 3_2^y)$; E_x': 3_1^x and $[1/2^{1/2}](3_2^x - 3_2^y)$; and E_y': 3_1^y and $-3_1^x 3_1^y$. (The minus sign on $-3_1^x 3_1^y$ is required for correct "orientation".) Being of A_1' symmetry, H_o^{2m} only permits intrapair couplings. The H_o^{2m} matrix is therefore composed of three 2×2 matrices, the eigenvectors for which are trivially obtained as

$$\begin{aligned}
E_{o,gs}^{2m} &= 0.0 \quad \nu_{gs} = 0_0 \\
E_{o,x}^{2m} &= 1399.2 \quad \nu_x = c_1\ 3_1^x + c_2\frac{1}{\sqrt{2}}[3_2^x - 3_2^y] \\
E_{o,y}^{2m} &= 1399.2 \quad \nu_y = c_1\ 3_1^y - c_2 3_1^x 3_1^y \\
E_{o,2x}^{2m} &= 2821.7 \quad 2\nu_x = -c_2\ 3_1^x + c_1\frac{1}{\sqrt{2}}[3_2^x - 3_2^y] \\
E_{o,2y}^{2m} &= 2821.7 \quad 2\nu_y = -c_2\ 3_1^y - c_1 3_1^x 3_1^y \\
E_{o,2A}^{2m} &= 2813.9 \quad 2\nu_A = \frac{1}{\sqrt{2}}[3_2^x + 3_2^y] \\
& c_1 = 0.9973, \quad c_2 = 0.0739
\end{aligned} \tag{13}$$

We use ν's to refer to eigenstates henceforth; $2\nu_x$ refers to an overtone state of E_x' symmetry. The expansion coefficients, c_1 and c_2, are the same for the E_x' and E_y' states, as per symmetry requirements. Note that c_2 depends on f, the cubic anharmonicity constant

$$c_2 \approx -\frac{3f}{\sqrt{2}\omega} \qquad f < 0 \tag{14}$$

The states in eq 13 form our core sextet of eigenstates upon which much of our analysis is based; we shall consider their all-mode versions in section 4.

The simple structure of the sextet of eigenvectors in eq 13 affords an easy, rapid computation of the time-dependent two-mode Hamiltonian with them

$$\mathbf{H}^{2m}(t) \approx \left[\begin{array}{c|cc|cc|c} 0 & -\frac{1}{\sqrt{2}}c_1F_x & -\frac{1}{\sqrt{2}}c_1F_y & \frac{1}{\sqrt{2}}c_2F_x & \frac{1}{\sqrt{2}}c_2F_y & 0 \\ \hline -\frac{1}{\sqrt{2}}c_1F_x & E^{2m}_{o,x}-\sqrt{2}c_1c_2F_x & \sqrt{2}c_1c_2F_y & -\frac{1}{\sqrt{2}}(c_1^2-c_2^2)F_x & \frac{1}{\sqrt{2}}(c_1^2-c_2^2)F_y & -\frac{1}{\sqrt{2}}c_1F_x \\ -\frac{1}{\sqrt{2}}c_1F_y & \sqrt{2}c_1c_2F_y & E^{2m}_{o,y}+\sqrt{2}c_1c_2F_x & +\frac{1}{\sqrt{2}}(c_1^2-c_2^2)F_y & \frac{1}{\sqrt{2}}(c_1^2-c_2^2)F_x & -\frac{1}{\sqrt{2}}c_1F_y \\ \hline \frac{1}{\sqrt{2}}c_2F_x & -\frac{1}{\sqrt{2}}(c_1^2-c_2^2)F_x & \frac{1}{\sqrt{2}}(c_1^2-c_2^2)F_y & E^{2m}_{o,2x}+\sqrt{2}c_1c_2F_x & -\sqrt{2}c_1c_2F_y & \frac{1}{\sqrt{2}}c_2F_x \\ \frac{1}{\sqrt{2}}c_2F_y & +\frac{1}{\sqrt{2}}(c_1^2-c_2^2)F_y & \frac{1}{\sqrt{2}}(c_1^2-c_2^2)F_x & -\sqrt{2}c_1c_2F_y & E^{2m}_{o,2y}-\sqrt{2}c_1c_2F_x & \frac{1}{\sqrt{2}}c_2F_y \\ 0 & -\frac{1}{\sqrt{2}}c_1F_x & -\frac{1}{\sqrt{2}}c_1F_y & \frac{1}{\sqrt{2}}c_2F_x & \frac{1}{\sqrt{2}}c_2F_y & E^{2m}_{o,2A} \end{array}\right] \tag{15}$$

The row/column ordering employed is the same as the order of states in eq 13. Of interest here are the excitation energies of the fundamentals that arise from the solution of this matrix. Showing that the $H^{2m}(t)$ matrix elements are adequate for this purpose is equivalent to stating that the sextet in eq 13 suffices. A key aspect in our rationalization is that the linear terms that make up $\delta V^{2m}(t)$ can couple harmonic basis functions that differ by only one quantum of excitation, which we will call $\Delta v = 1$ coupling.

The boxed $\nu_x-\nu_y$ block of $\mathbf{H}^{2m}(t)$ in eq 15 shows the solvent-induced coupling between these two states. We shall soon see that the mean eigenvalue splitting is mainly due to this block. All four terms involve a common prefactor of $2^{1/2}c_1c_2$, which, using the states' expansions, is seen to arise from the couplings between one and two quantum basis functions. Since only such $\Delta v = 1$ couplings are permitted by the form of $\delta V^{2m}(t)$ (eq 5), the involvement of three and higher quantum functions, when included, will be weak.[21]

Further, the $2^{1/2}c_1c_2$ prefactor itself will remain essentially constant regardless of the length of the eigenfunction expansions. From a perturbation theoretic viewpoint, $c_1 \approx 1$, and c_2 would be nearly unchanged even if a larger harmonic basis were used to diagonalize H_o^{2m}. Put together, one sees that the small, six-function basis captures the main contributions in the intrafundamental matrix elements.

These arguments may be extended to state that, in eq 15, the rest of the second and third rows/columns, and even the first row/column for the ground state's couplings, are practically converged for the chosen solute−solvent coupling, $\delta V(t)$. (Since we desire excitation energies, the ground state must be given due attention.) We point out that the lack of higher anharmonicities in H_o^{2m}, or the small energy differences between truly converged states and those used here, cause only minor numerical changes.

By the same token, for the bottom-right, 3×3 overtone block in eq 15, it will take the second overtone to incorporate all of the key solvent effects. While we shall err in the energies of the overtones, this will not be a impediment to our targets. The imprecision will be much smaller than the fundamental−overtone energy gap; moreover, this gap is also at least 10 times larger than the couplings between the two state sets.

3.3. Two-Mode Quantum Treatment: Asymmetric Stretch Excitation Energies, Their Distributions, and Splitting. We now move on to solving $\mathbf{H}^{2m}(t)$ for the fundamental energies. To reduce the clutter of coefficients in the following, all off-block diagonal occurences of c_1 and $c_1^2-c_2^2$ in eq 15 are set to unity. The $2^{1/2}c_1c_2$ prefactor common to the $\nu_x-\nu_y$ as well as the $2\nu_x-2\nu_y$ blocks cannot be reduced. However, with $c_1 \approx 1$

$$\sqrt{2}c_1c_2 \approx -\frac{3f}{\omega} = \alpha \tag{16}$$

where we have used eq 7. We thus replace the force prefactors of both 2×2 blocks by α, so that they have the structure

$$\pm\begin{bmatrix} -\alpha F_x & \alpha F_y \\ \alpha F_y & \alpha F_x \end{bmatrix}$$

We have already encountered this matrix in the classical treatment of section 3.1. We reuse the rotation matrix, $\mathbf{R}(t)$, eq 8, to define a larger matrix

$$\mathbf{U(t)} = \begin{bmatrix} 1 & \mathbf{0} & \mathbf{0} & 0 \\ \mathbf{0} & \mathbf{R(t)} & \mathbf{0} & \mathbf{0} \\ \mathbf{0} & \mathbf{0} & \mathbf{R(t)} & \mathbf{0} \\ 0 & \mathbf{0} & \mathbf{0} & 1 \end{bmatrix} \tag{17}$$

Applying this to eq 15, we obtain

$$\mathbf{U}(t)^T\mathbf{H}^{2m}(t)\mathbf{U}(t) \approx \left[\begin{array}{c|cc|ccc} 0 & -\frac{1}{\sqrt{2}}F\cos\frac{3}{2}\theta & -\frac{1}{\sqrt{2}}F\sin\frac{3}{2}\theta & 0 & 0 & 0 \\ \hline -\frac{1}{\sqrt{2}}F\cos\frac{3}{2}\theta & \omega-\alpha F & 0 & -\frac{1}{\sqrt{2}}F & 0 & -\frac{1}{\sqrt{2}}F\cos\frac{3}{2}\theta \\ -\frac{1}{\sqrt{2}}F\sin\frac{3}{2}\theta & 0 & \omega+\alpha F & 0 & \frac{1}{\sqrt{2}}F & -\frac{1}{\sqrt{2}}F\sin\frac{3}{2}\theta \\ \hline 0 & -\frac{1}{\sqrt{2}}F & 0 & 2\omega+\alpha F & 0 & \frac{1}{\sqrt{2}}c_2F\cos\frac{3}{2}\theta \\ 0 & 0 & \frac{1}{\sqrt{2}}F & 0 & 2\omega-\alpha F & \frac{1}{\sqrt{2}}c_2F\sin\frac{3}{2}\theta \\ 0 & -\frac{1}{\sqrt{2}}F\cos\frac{3}{2}\theta & -\frac{1}{\sqrt{2}}F\sin\frac{3}{2}\theta & \frac{1}{\sqrt{2}}c_2F\cos\frac{3}{2}\theta & \frac{1}{\sqrt{2}}c_2F\cos\frac{3}{2}\theta & 2\omega \end{array}\right] \quad (18)$$

We have made two unannounced changes in this matrix. First, the ground state−overtone coupling $(1/2^{1/2})c_2F_{x(y)}$ is set to 0 as it is much smaller than their energy gap. Second, we have replaced all diagonal fundamental and overtone energies by their respective harmonic counterparts, ω and 2ω. This latter approximation is in keeping with our assertion at the end of section 3.2 that we need neither exact overtone energies nor exact energy gaps between the three sets of states that make up $\mathbf{H}^{2m}(t)$. In the same vein, we now neglect the intraovertone couplings in the last row and column in eq 18.

That done, the remaining structure of the transformed matrix permits us to treat the couplings of the fundamentals to the ground and overtone states in a pairwise perturbative manner. We thereby write down for the upper (E_u) and lower (E_l) state energies

$$E_{\mathrm{l}} \approx \left(\begin{array}{c} \omega-\alpha F+\dfrac{\frac{1}{2}F^2\cos^2\frac{3}{2}\theta}{\omega-\alpha F}-\dfrac{\frac{1}{2}F^2}{\omega+2\alpha F} \\ -\dfrac{\frac{1}{2}F^2\cos^2\frac{3}{2}\theta}{\omega+\alpha F}+\dfrac{\frac{1}{2}F^2\cos^2\frac{3}{2}\theta}{\omega-\alpha F}+\dfrac{\frac{1}{2}F^2\sin^2\frac{3}{2}\theta}{\omega+\alpha F} \end{array}\right)$$

$$\approx \omega-\alpha F+\frac{\alpha F^3\left[1+\cos^2\frac{3}{2}\theta\right]}{\omega^2}+\frac{\frac{1}{2}\alpha F^3\cos 3\theta}{\omega^2}$$

$$E_{\mathrm{u}} \approx \left(\begin{array}{c} \omega+\alpha F+\dfrac{\frac{1}{2}F^2\sin^2\frac{3}{2}\theta}{\omega+\alpha F}-\dfrac{\frac{1}{2}F^2}{\omega-2\alpha F} \\ -\dfrac{\frac{1}{2}F^2\sin^2\frac{3}{2}\theta}{\omega-\alpha F}+\dfrac{\frac{1}{2}F^2\cos^2\frac{3}{2}\theta}{\omega-\alpha F}+\dfrac{\frac{1}{2}F^2\sin^2\frac{3}{2}\theta}{\omega+\alpha F} \end{array}\right)$$

$$\approx \omega+\alpha F-\frac{\alpha F^3\left[1+\sin^2\frac{3}{2}\theta\right]}{\omega^2}+\frac{\frac{1}{2}\alpha F^3\cos 3\theta}{\omega^2} \quad (19)$$

The last two terms of the bracketed expressions for E_l and E_u are simply the subtracted value of the ground-state energy. Note that, to zeroth order in α, the downward "push" of the A_1' overtone cancels the upward "push" of the fundamentals by the ground state (first two $\sin^2$ terms in E_u, first two $\cos^2$ terms in E_l). The resulting splitting to first order in the anion−solvent coupling coefficient, α (eq 16), is

$$\Delta E_{\mathrm{sp}} = E_{\mathrm{u}} - E_{\mathrm{l}} \approx 2\alpha F - 3\alpha\frac{F^3}{\omega^2} \quad (20)$$

With the harmonic frequency, ω, typically being an order of magnitude larger than F, the second term here contributes only slightly to the splitting. In fact, this also allows us to state that

$$E_{\mathrm{u}} \approx \omega + \alpha F \qquad E_{\mathrm{l}} \approx \omega - \alpha F \quad (21)$$

The dominant contribution to the fundamental excitation energies and the splitting therefore comes from the $\nu_x-\nu_y$ block of $\mathbf{H}^{2m}(t)$ in eq 15.

Equation 21 is essentially eq 10 of the previous classical analysis. This indicates that the distributions of the E_u and E_l from the above quantum treatment of $H^{2m}(t)$, which we will call $\rho(E_{u,l})$, will be rather similar to the spread of harmonic frequencies in the classical analysis. We make this comparison in Figure 3. The red curve for the binned distribution of E_u and E_l was directly obtained from the diagonalization of the $H^{2m}(t)$ matrix in eq 15. The water solvent forces were taken from the simulations. Note that this Hamiltonian matrix uses the actual fundamental energies of the two-mode eigenstates (1399.2 cm^{-1}), rather than approximating them as ω (= 1407.0 cm^{-1}). The black curve is that in Figure 2 and represents the spread of values for either the classical harmonic frequencies or the (E_u, E_l) pair of eq 21. (The center of the black curve has been shifted by 1399.2 − 1407.0 = −7.8 cm^{-1}.) As expected, the two distributions are very much alike. The mean value of the splitting for the red curve, $\Delta E_{\mathrm{sp}} = \langle E_u - E_l\rangle$, is 24.4 cm^{-1}, which is very close to 23.8 cm^{-1} for the black curve.[22]

To complete the two-mode analysis, we consider the influence of the force gradients, G_{ij}, that have been so far ignored in the quantum treatment. Upon their inclusion in the 2m Hamiltonian, the fundamental excitation energies are found distributed as in the gray curve of Figure 3. The change in shape from the red curve is small, and the new mean splitting is only augmented by 0.8 to 25.2 cm^{-1}. Yet again, we find little gain from the force gradients for the state energies and their distribution.

We will now turn to a more detailed and accurate description of the eigenvalue distribution and mean splitting. Remarkably, and contrary to our initial expectations, the numerical impact on the splitting estimation above is minimal, with some modest distortions to the distribution shapes in the more sophisticated analyses.

4. Six-Mode Analysis

We have demonstrated thus far that the treatment of the two NO asymmetric stretch modes alone is a quite useful approach to nitrate symmetry breaking. We now begin an examination of the effect of the other four modes of the anion. All intramolecular couplings in V_{anh} need to be introduced into the problem, which requires the computation of the all-mode eigenstates of the molecular Hamiltonian, H_o. This is the subject of section 4.1. With these eigenvectors in hand, we now have two variables to control in the solute−solvent coupling approach,

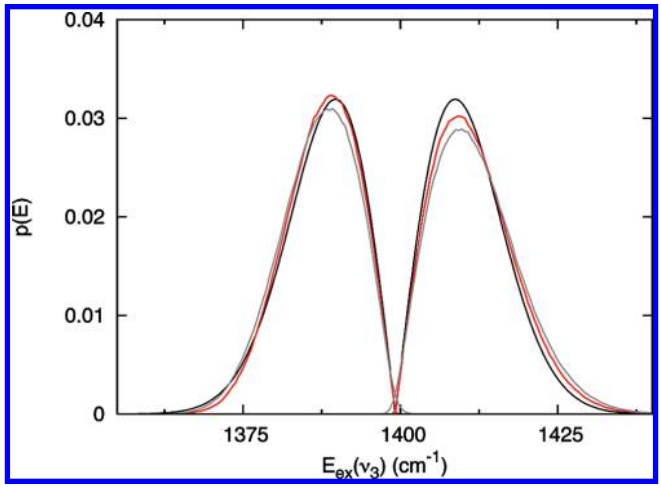

Figure 3. Distribution of NO asymmetric stretch fundamental excitation energies obtained from a direct solution of the two-mode matrix in eq 15 using simulation NO_3^-−H_2O forces (red) and from an expanded form of the same matrix with nitrate−water force gradients included (gray). In black is the curve from Figure 2, which is the plot of the spread of the split frequencies in eq 10 or, equally, the split energies of eq 21. Its center has been shifted by −7.8 cm^{-1} to align it with the other curves.

namely, the size of the eigenbasis used for the full time-dependent Hamiltonian, $H(t)$, and the set of anion−water solvent forces, F_i, included. Our approach will be that of a progressive switch from a two-mode-like to a six-mode analysis, which we present in sections 4.2 and 4.3. We shall present the distributions of excitation energies, $\rho(E_{u,I})$, and mean splittings, ΔE_{sp}, for the NO asymmetric stretch fundamentals at each stage.

4.1. Six-Mode Eigenstates. The first task at hand is the diagonalization of H_o of eq 1. As in the two-mode case, we employ a harmonic basis. We will use the notation $a_m^x b_n$ to mean a basis function with m quanta of vibrational excitation in mode Q_{ax} and n in Q_b. Of course, the unindicated modes are at their zero-point levels. The x or y superscripts apply to the asymmetric stretches and in-plane bends alone (modes 3 and 4). A raw basis composed of such functions is symmetrized via linear combinations and is sorted into eight subsets, one for each of the eight D_{3h} symmetry species. Since H_o can only couple basis functions within a given subset, the task of diagonalization is greatly simplified.[23] It remains only to choose an adequately large basis of each symmetry type to converge the necessary eigenstates. We find that a harmonic energy cutoff of 10000 cm^{-1} (relative to the ground-state function, 0_0) is sufficient to converge all states below about 4000 cm^{-1}. Attesting to this are the mean absolute differences of 0.9 and 0.2 cm^{-1} of the energies of these states from those computed with a basis cutoff of 9000 and 12000 cm^{-1}. The energies and description of the ground, fundamental, and some overtone states are shown in Table 2. The label $m\nu_a$ refers to an eigenstate that is predominantly like a symmetrized basis function with m quanta in mode Q_a. Additional tags or subscripts serve to specify the symmetry.

Some aspects of these state expansions deserve mention. Note, first, that the NO symmetric stretch permeates all of them. Functions like 1_1 or 1_1m_n are the second most important in the lists. Their presence can be traced back to potential terms of the form $Q_1Q_2^2$, $Q_1(Q_{3x}^2 + Q_{3y}^2)$, and $Q_1(Q_{4x}^2 + Q_{4y}^2)$. (The last ones for the in-plane bends can be thought of as a Fermi coupling.) Changing Q_1 means uniformly changing all three NO bond lengths, and such cubic terms simply express the dependence of the harmonic frequencies and, thereby, other computed properties on the bond length.

Placed only about 75 cm^{-1} above the asymmetric stretch fundamentals, ν_{3x} and ν_{3y}, are the bend overtone states, $2\nu_{4x}$ and $2\nu_{4y}$. The two pairs are not strongly coupled, despite the proximity; 3_1^x and 3_1^y have a coefficient of 0.034 in the expansions of the bend overtones and vice versa. This weak intermolecular coupling is corroborated by the absence of an "intensity shared" peak in the vicinity of 1450 cm^{-1}.[24]

4.2. Progressive Inclusion of Water Solvent-Induced Effects on the Core Sextet. In the two-mode quantum treatment in sections 3.2 and 3.3, we saw that applying the solute−solvent coupling scheme with the sextet

$$\{\nu_{gs}, \nu_{3x}, \nu_{3y}, 2\nu_{3x}, 2\nu_{3y}, 2\nu_{3A}\} \tag{22}$$

was sufficient to capture the solvent effects on the two NO asymmetric stretch fundamentals, ν_{3x} and ν_{3y}. We restart from that very point, only switching to the six-mode (6m) versions of these eigenstates. In the next three subsections, we study the changes to the energies of the ν_3 fundamentals as we introduce, stepwise, the solvent forces on the six modes.

The following dissection of the solvent-induced coupling will be useful in the analyses. Writing the eigenstates as $|\psi_i\rangle = \sum_k c_{ki}|\phi_k\rangle$, where $|\phi_k\rangle$ are the symmetrized harmonic basis functions, we obtain

$$\delta V_{ij}(t) = -\sum_m F_m \sum_{kl} c_{ki}c_{lj}(Q_m)_{kl} \tag{23}$$

Here, $(Q_m)_{kl} = \langle\phi_k|Q_m|\phi_l\rangle$, which are trivially evaluated. The coefficient products are, of course, a reflection of the intramolecular couplings. For a given force, F_m, usually only a few terms of the bracketed sum need to be considered. This is profitable in two ways. (1) We can make estimates of the coupling sizes between a state pair. Whether the two states affect each other significantly or not may be judged in a perturbative fashion. If they do, (2) we try to identify, through the $|\phi_k\rangle$,$|\phi_l\rangle$ pairs involved, the terms in V_{anh} that gave rise to the key summands. We thereby gain a clearer, physical understanding of the effect of each F_m on the state pair under investigation.

4.2.1. Effect of the Solvent Forces on the Asymmetric Stretches. We start with a check. If we were to retain the two-mode form of the solute−solvent coupling

$$\delta V(t) \equiv \delta V^{2m}(t) = -F_{3x}Q_{3x} - F_{3y}Q_{3y} \tag{24}$$

the presence of the other modes and the larger size of the expansions of the sextet (eq 22) should not matter. The reason for this is that we effectively return to the 2m case of section 3.2. The expansion functions 3_1^x, 3_1^y, $(1/2^{1/2})(3_2^x - 3_2^y)$ and $-3_1^x3_1^y$, which made up the 2d eigenstates in eq 13, remain the major role players in generating the solvent-induced couplings. Furthermore, the coefficients of these four basis functions in the new, all-mode expansions of ν_{3x} and ν_{3y} (Table 2) are only slightly different from their 2m counterparts.

In summary, we expect the $H(t)$ matrix to be essentially unchanged from its 2m form in eq 15.[25] This would, in turn, generate nearly the same excitation energy distribution, $\rho(E_{u,I})$, and mean eigenvalue splitting, ΔE_{sp}, that we obtained in the 2m treatment. Figure 4 compares the two distributions. The red line is the 2m result that has been carried over from Figure 3, while the black line is for the 6m counterpart. (Note that the red curve has been shifted to account for the 2m to 6m

TABLE 2: A Few Eigenvectors[a] of the Full Six-Mode NO_3^- Hamiltonian, H_o, and Their Energies in cm^{-1}

0.0	ν_{gs}	726.1	ν_{4x}	ν_{4y}
0.9912	0_0	0.9883	4_1^x	4_1^y
0.1266	1_1	0.1442	$1_14_1^x$	$1_14_1^y$
0.0217	$\frac{1}{\sqrt{2}}(1_13_2^x+1_13_2^y)$	0.0183	$\frac{1}{\sqrt{2}}(4_2^x-4_2^y)$	$-4_1^x4_1^y$
0.0113	1_2	−0.0135	$1_13_1^x$	$1_13_1^y$
		−0.0116	$\frac{1}{\sqrt{2}}(3_2^x-3_2^y)$	$-3_1^x3_1^y$
821.4	$\nu_2(A_2'')$			
0.9918	2_1	1376.5	ν_{3x}	ν_{3y}
0.1216	1_12_1	0.9720	3_1^x	3_1^y
		0.1991	$1_13_1^x$	$1_13_1^y$
1046.9	$\nu_1(A_1')$	0.0699	$\frac{1}{\sqrt{2}}(3_2^x-3_2^y)$	$-3_1^x3_1^y$
0.9634	1_1	−0.0525	$1_14_1^x$	$1_14_1^y$
0.2173	1_2	−0.0456	$\frac{1}{\sqrt{2}}(3_1^x4_1^x-3_1^y4_1^y)$	$-\frac{1}{\sqrt{2}}(4_1^x3_1^y+3_1^x4_1^y)$
−0.1267	0_0	0.0343	$\frac{1}{\sqrt{2}}(4_2^x-4_2^y)$	$-4_1^x4_1^y$
0.0462	$\frac{1}{\sqrt{2}}(4_2^x+4_2^y)$	0.0153	4_1^x	4_1^y
0.0461	$\frac{1}{\sqrt{2}}(3_2^x+3_2^y)$			
−0.0291	$\frac{1}{\sqrt{2}}(3_1^x4_1^x+3_1^y4_1^y)$	1452.0	$2\nu_{4x}$	$2\nu_{4y}$
		0.9842	$\frac{1}{\sqrt{2}}(4_2^x-4_2^y)$	$-4_1^x4_1^y$
1451.8	$2\nu_4(A_1')\equiv 2\nu_{4A}$	0.1615	$\frac{1}{\sqrt{2}}(1_14_2^x-1_14_2^y)$	$-1_14_1^x4_1^y$
0.9832	$\frac{1}{\sqrt{2}}(4_2^x+4_2^y)$	−0.0344	3_1^x	3_1^y
0.1610	$\frac{1}{\sqrt{2}}(1_14_2^x+1_14_2^y)$	0.0256	$\frac{\sqrt{3}}{2}4_3^x+\frac{1}{2}4_1^x4_2^y$	$\frac{\sqrt{3}}{2}4_3^y+\frac{1}{2}4_2^x4_1^y$
−0.0473	1_1	−0.0191	4_1^x	4_1^y
0.0444	$\frac{1}{2}4_3^x-\frac{\sqrt{3}}{2}4_1^x4_2^y$	−0.0188	$\frac{1}{\sqrt{2}}(1_13_1^x4_1^x-1_13_1^y4_1^y)$	$-\frac{1}{\sqrt{2}}(1_14_1^x3_1^y+1_13_1^x4_1^y)$
−0.0187	$\frac{1}{\sqrt{2}}(1_13_1^x4_1^x+1_13_1^y4_1^y)$	−0.0164	$\frac{1}{2}(3_2^x4_1^y-4_1^x3_2^y)+\frac{1}{\sqrt{2}}3_1^x3_1^y4_1^y$	$-\frac{1}{2}(3_2^x4_1^y-3_2^y4_1^y)+\frac{1}{\sqrt{2}}3_1^x4_1^x3_1^y$
−0.0165	$\frac{1}{2}(3_2^x4_1^x-4_1^x3_2^y)-\frac{1}{\sqrt{2}}3_1^x3_1^y4_1^y$			
−0.0103	1_2	2752.2	$2\nu_{3x}$	$2\nu_{3y}$
		0.9442	$\frac{1}{\sqrt{2}}(3_2^x-3_2^y)$	$-3_1^x3_1^y$
2725.6	$2\nu_3(A_1')\equiv 2\nu_{3A}$	0.2626	$\frac{1}{\sqrt{2}}(1_13_2^x-1_13_2^y)$	$-1_13_1^x3_1^y$
0.9366	$\frac{1}{\sqrt{2}}(3_2^x+3_2^y)$	0.0941	$\frac{\sqrt{3}}{2}3_3^x+\frac{1}{2}3_1^x3_2^x$	$\frac{\sqrt{3}}{2}3_3^y+\frac{1}{2}3_2^x3_1^y$
0.2590	$\frac{1}{\sqrt{2}}(1_13_2^x+1_13_2^y)$	−0.0672	$\frac{1}{\sqrt{2}}(1_13_1^x4_1^x-1_13_1^y4_1^y)$	$-\frac{1}{\sqrt{2}}(1_14_1^x3_1^y+1_13_1^x4_1^y)$
0.1616	$\frac{1}{2}3_3^x-\frac{\sqrt{3}}{2}3_1^x3_2^y$	−0.0655	3_1^x	3_1^y
−0.0815	$\frac{1}{2}(3_2^x4_1^x-4_1^x3_2^y)-\frac{1}{\sqrt{2}}3_1^x3_1^y4_1^y$	0.0650	$\frac{1}{\sqrt{2}}4_1^x3_1^y4_1^y+\frac{1}{2}(3_1^x4_2^x-3_1^x4_2^y)$	$\frac{1}{\sqrt{2}}3_1^x4_1^x4_1^y-\frac{1}{2}(4_2^x3_1^y-3_1^y4_2^y)$
−0.0596	$\frac{1}{\sqrt{2}}(1_13_1^x4_1^x+1_13_1^y4_1^y)$	−0.0642	$\frac{1}{\sqrt{2}}(3_2^x4_1^x+4_1^x3_2^y)$	$\frac{1}{\sqrt{2}}(3_2^x4_1^y+3_2^y4_1^y)$
0.0489	$\frac{1}{\sqrt{2}}(3_1^x4_1^x+3_1^y4_1^y)$	−0.0428	$1_13_1^x$	$1_13_1^y$
−0.0453	1_1	0.0267	$\frac{1}{\sqrt{2}}(3_1^x4_1^x-3_1^y4_1^y)$	$-\frac{1}{\sqrt{2}}(4_1^x3_1^y+3_1^x4_1^y)$
0.0324	$\frac{1}{2}(3_1^x4_2^x-3_1^x4_2^y)-\frac{1}{\sqrt{2}}4_1^x3_1^y4_1^y$	−0.0135	$1_23_1^x$	$1_23_1^y$
−0.0215	1_2	0.0112	4_1^x	4_1^y
		0.0100	$1_24_1^x$	$1_24_1^y$

[a] The expansions have been restricted to one quantum of excitation higher than the leading basis function, even if higher basis functions have coefficients larger than 0.01.

reference eigenvalue change for ν_3.) The agreement of the two curves depicts our assertion. The ν_3 splitting, ΔE_{sp}, is 24.5 cm^{-1}, while that for the black curve is 24.4 cm^{-1}.

4.2.2. Effect of the Solvent Forces on the In-Plane Bends. Next, we update $\delta V(t)$ in eq 24 by including also the solvent forces on the in-plane bends, that is, $-F_{4x}Q_{4x} - F_{4y}Q_{4y}$. Recomputing the $H(t)$ matrix with the core sextet, the spreads of the E_u and E_l now appear as the green curve in Figure 4. It has a smaller width than the red curve of the previous step. Though not dramatic, an analysis of the effect of the F_4's shall prove insightful.

These new additions to $\delta V(t)$ can couple basis functions that differ by one quantum in the in-plane bends. Using eq 23 with the core sextet's expansions in Table 2, we estimate that the existing coupling between the fundamentals and the other four states is revised by 1−2 cm^{-1}. The change is not significant compared to the energy gap between the states in question. It will therefore suffice to focus on how the two in-plane bend forces affect the ν_{3x}−ν_{3y} pair alone.

Sifting through the basis functions of the fundamental state pair, one finds that $-F_{4x}Q_{4x} - F_{4y}Q_{4y}$ can couple 3_1^x and 3_1^y to $(1/2^{1/2})(3_1^x4_1^x - 3_1^y4_1^y)$ and $(-1/2^{1/2})(4_1^x3_1^y + 3_1^x4_1^y)$ and that these give rise to the dominant additions to the ν_{3x}−ν_{3y} couplings. The latter two basis functions, which we label as $|a_x\rangle$ and $|a_y\rangle$, appear in the ν_{3x} and ν_{3y} expansions with the same coefficients $c_b = -0.0456$. The coupling structure that results adds the following to the 2 × 2 fundamental block of eq 15

$$-2c_1|c_b|\begin{bmatrix}\langle 3_1^x|\delta V|a_x\rangle & \langle 3_1^x|\delta V|a_y\rangle\\ \langle 3_1^y|\delta V|a_x\rangle & \langle 3_1^y|\delta V|a_y\rangle\end{bmatrix} = -c_1|c_b|\begin{bmatrix}-F_{4x} & F_{4y}\\ F_{4y} & F_{4x}\end{bmatrix} \tag{25}$$

We have already encountered a coupling matrix of this structure in the two-mode subproblem; see eq 9. At that point, the matrix afforded the classical interpretation that the solvent forces, working through the anharmonicity, altered the NO asymmetric stretch harmonic frequencies, ω_3. Looking for a similar explanation in the current instance, we trace back the presence of $|a_{x(y)}\rangle$ in the $\nu_{3x(y)}$ expansions to the cubic potential term

$$f'[(Q_{3x}^2 - Q_{3y}^2)Q_{4x} - 2Q_{3x}Q_{3y}Q_{4y}] \tag{26}$$

This term is a reflection, in part, of the fact that the in-plane bend and asymmetric stretch normal modes are both admixtures

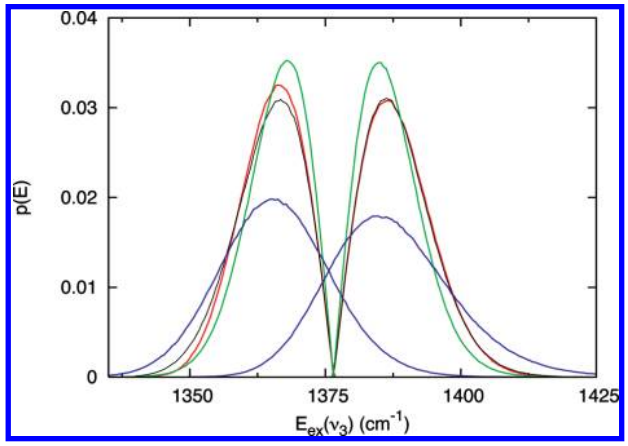

Figure 4. Distribution of NO asymmetric stretch excitation energies obtained from the core sextet of 6m eigenstates. The red curve is a 2m result, and is a repeat of the trace of the same color in Figure 3. Its center has been shifted by the difference between the 2m and 6m ν_3 reference eigenvalues, which aligns it with the other curves in the plot. The black curve was obtained with the solvent forces limited to only the forces on the title mode pair. Adding the effect of the in-plane bend forces yielded the green curve. Using all six forces yielded the blue curve.

of the bond angle and bond length changes. Following the same completion-of-squares pathway of section 3.1, but now applied to the in-plane bends, we find the additions to the asymmetric stretch harmonic potential to be proportional to eq 25 above. In this manner, the solvent forces on the in-plane bends contribute to the modulation of ω_3.

In the quantum treatment, the total coupling at this stage between ν_{3x} and ν_{3y} is equal to the sum of eq 25 and the boxed 2×2 matrix in eq 15. The new excitation energies are then

$$E_{u,l} = E_o(\nu_3) + \sqrt{(\alpha F_{3x} - c_1|c_b|F_{4x})^2 + (\alpha F_{3y} - c_1|c_b|F_{4y})^2} \quad (27)$$

where $E_o(\nu_3)$ is the unperturbed $\nu_{3x(y)}$ energy. Given the form of this expression, it is difficult to make a prediction about the direction in which the mean splitting changes due to the in-plane bend forces. Simulation data comes to our aid. As noted in Appendix B, (F_{3x},F_{4x}) and (F_{3y},F_{4y}) have a normalized covariance of 0.475. With this information and the relative sign of F_3 and F_4 terms under the square root in eq 27, a reduction of the splitting is expected. Indeed, the new splitting is 21.6 cm^{-1} for the green curve in Figure 4, a notable change from 24.5 cm^{-1} without the in-plane bends (red curve in the figure).

4.2.3. Effect of the Solvent Force on the Symmetric Stretch. Finally, we include in the anion−solvent interaction the forces on the symmetric stretch (Q_1) and out-of-plane (Q_2) modes. Since Q_2 is of A_2'' symmetry, $-F_2Q_2$ cannot couple any pair in the core sextet (eq 22). On the other hand, $-F_1Q_1$ can only affect those of the same symmetry. This keeps the couplings largely diagonal; the off-diagonal couplings are perturbatively weak within the sextet. For the diagonal couplings, $\delta V_{ii}(t)$, the main expansion term in each of them is of the form

$$-\beta\langle 1_1a_m|(F_1Q_1)|a_m\rangle = -\frac{1}{\sqrt{2}}\beta F_1 \quad (28)$$

with a_m being the leading basis function for the ith state of the sextet, and $\beta \approx c(1_1a_m)$, the coefficient of 1_1a_m in the same expansion. The shift magnitude and direction is the same for the two ν_3 fundamentals. With the absence of a differential effect, there should be no further change in the mean splitting. Indeed, its computed value is 21.6 cm^{-1}. The new energy spread, $\rho(E_{u,l})$, plotted in blue in Figure 4, is rather flattened compared to the green curve of the previous step, though the peak positions are roughly the same.

In view of the other three curves of Figure 4, the breadth of this new one is a bit odd. We have just stated that the symmetric stretch force does not add to the splitting of the ν_3 states, but it certainly moves their absolute positions together. What we have forgotten is the ground state, the reference level relative to which E_u and E_l are measured. If $-F_1Q_1$ moves the position of the ground state to a lesser (or larger) extent than the fundamentals, an increase of width may be expected.

To begin checking on this explanation, we identify V_{anh} terms though which the symmetric stretch force can act on the ν_{gs} and the ν_3's. These are

$$f_1Q_1^3 \qquad f_2Q_1Q_2^2 \qquad f_3Q_1(Q_{3x}^2 + Q_{3y}^2) \qquad f_4Q_1(Q_{4x}^2 + Q_{4y}^2) \quad (29)$$

where $f_1 \approx -32$, $f_2 \approx 6$, $f_3 \approx -123$, and $f_4 \approx -28$ cm^{-1}. These terms briefly appeared at the end of section 4.1. Physically, each of these express the NO bond length dependence for the harmonic frequencies of all of the nitrate modes. This can be expressed as $\omega_i' \approx \omega_i + f_iQ_1$, where we have reused the procedure of eq 10.[26] The energy of a harmonic level is thereby changed from $\sum_i \omega_i(v_i + 1/2)$ by an amount $\sum_i f_i(v_i + 1/2)Q_1$, while excitation energies are changed by $\sum_i f_i v_i Q_1$. In words, the energy of a mode is more affected by a bond length change if it is already excited. Thus, for the Q_3 modes, the (harmonic) one quantum level varies by f_3Q_1 more than the (harmonic) ground level. Given that $f_3 \approx -123$ cm^{-1}, this will be an important difference.[27]

Returning to the quantum picture of eq 28, the f_3Q_1 difference would be reflected in a larger coefficient for $1_13_1^{x(y)}$ in $\nu_{3x(y)}$ than for 1_1 in the ground state. Indeed, their values in Table 2 are 0.2 and 0.127, respectively. This would, in turn, cause a larger shift of the diagonal matrix element for the fundamentals than that for the ground state, resulting in a larger $\rho(E_{u,l})$ width. This is just what Figure 4 shows. The root of the effect is the cubic term with f_3 in eq 29. To numerically verify the above arguments, we have rerun the whole series of calculations with $f_3 = 0$. Though not shown, the distribution so obtained is no longer broadened and is quite close to the green curve in the figure.

4.3. Couplings to States beyond the Sextet. In implementing the switch from a two-mode to a full six-mode treatment of aqueous NO_3^-, we have so far restricted the number of eigenstates that we employ in the solute−solvent approach to the core sextet, eq 22. The investigation of the solvent-force-induced couplings among this set of states has led us to a result analogous to the two-mode one. The solvent forces on the anion's modes, through various intramolecular (cubic) anharmonicities, modulate the harmonic frequencies of the NO asymmetric stretches and hence their excitation energy distributions [$\rho(E_{u,l})$] and/or their mean splitting [ΔE_{sp}]. It remains to be discovered whether other eigenstates of NO_3^- could lead to any additional effects on these average quantities. We now address this final task.

Apart from the sextet, eq 22, states whose leading basis functions have up to 2 quanta of excitation are added. A few with 3 quanta are also included, limiting the state list to those

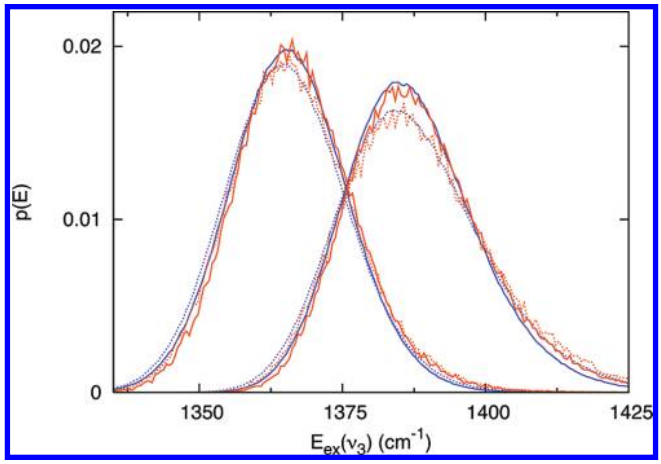

Figure 5. A plot comparing the ν_3 excitation energy distributions computed with the core 6m sextet of NO asymmetric stretch states (in blue) and with a much larger set of 6m eigenstates (in orange). The solid curves are for results obtained with a solute−solvent coupling that contains only solvent forces on the NO_3^-'s modes, while the dotted ones are for when we included the force gradients as well. See section 4.3 for details.

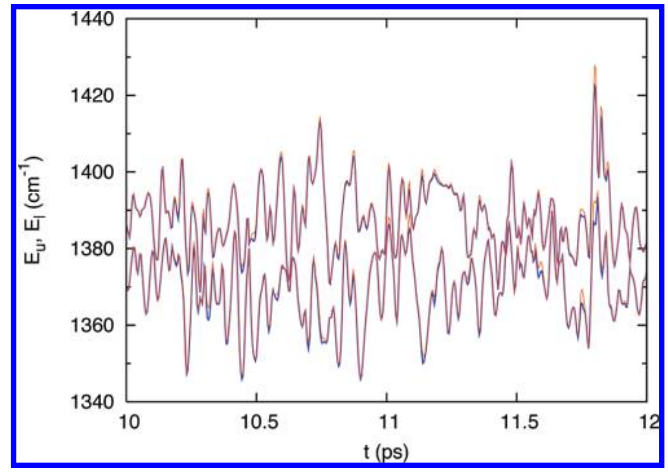

Figure 6. Trajectory plot of the excitation energies, $E_u(t)$ and $E_l(t)$, using the core 6m sextet (blue) and the expanded 6m eigenbasis (orange) with all solvent forces, F_i, included in the calculation.

that have at least 2 quanta in the in-plane and out-of-plane modes together. The states that fit this bill are 56 in number. For the moment, we do not attempt to organize them into rungs of importance.

Using this large set of eigenstates, we compute and diagonalize the matrix of $H(t)$ (eq 4). Out of the eigenvectors obtained at a given instance, we identify the pair that has the highest ν_{3x}, ν_{3y} character using a best match procedure.[28] Binning the energies (E_u, E_l) of this vector pair, we obtain the distributions in solid orange in Figure 5. The blue curve has been carried over from the previous figure (Figure 4) and represents the energy spread of the pure ν_3 vectors. The two curves hardly differ. (The noisiness of the orange curve is due to lower sampling.) The splitting, ΔE_{sp}, for the orange curve is 21.7 cm^{-1}, hardly different from the 21.6 cm^{-1} value for the blue curve. The dashed curves are obtained with the force gradients as well as the forces and are only slightly shorter and broader than their solid colored counterparts.

Apparently, all of the extra states do not cause any differential solvent-induced effect on the ν_3 fundamentals beyond what was already captured by the sextet. This is a curious result, which suggests either that the extra couplings are small and/or ineffectual or that they equally affect ν_{gs}, ν_{3x}, and ν_{3y}. Indeed, various extra-sextet states fall into one of these two categories, further details of which are presented in Appendix C.

These findings about the extra-sextet states motivate the statement that they have no new effect on the dynamics of the ν_3 excitation energies, $E_u(t)$ and $E_l(t)$, beyond what the core sextet generates in all-mode space. This is echoed in the time traces of the above two energies in Figure 6 computed with (orange) and without (blue) the states added in this section. Therefore, further analysis of symmetry breaking that deals explicitly with the time dependence of the NO asymmetric stretch fundamentals should be possible with just the core sextet, $\{\nu_{gs},\nu_{3x},\nu_{3y},2\nu_{3x},2\nu_{3y},2\nu_{3A}\}$. Our current efforts are in this direction.

5. Summary and Concluding Remarks

We have presented a first systematic, albeit initial, theoretical investigation into vibrational symmetry breaking of NO_3^- in aqueous solution. This effect arises from the degeneracy of the two NO asymmetric stretches of the anion being lost in solution. It is spectrally manifested in the appearance of two bands separated by about 35−60 cm^{-1} in the experimental infrared and Raman spectra in the 1350−1400 cm^{-1} region.[1,8−11] On the path to a direct comparison of theoretical spectra with experiments, this article has examined the dependence of the excitation energies of the two asymmetric stretch fundamentals on the forces exerted by the solvent on the anion's modes, with internal anion charge fluctuations,[13−15] among other aspects, left for future investigation.

Our analyses were carried out via the perturbative solute−solvent coupling approach. A reference Hamiltonian for the vibrations of NO_3^- was developed, and forces and force gradients that represent the solvent influence were then added to obtain a time-dependent Hamiltonian, $H(t)$. The time evolution of these added quantities were obtained from rigid molecular dynamics simulations, employing a NO_3^-−H_2O force field recently developed by Thomas et al.[18] By treating $H(t)$ at various levels of complexity, we have elucidated the role of the various solvent forces. In each of the analyses, the upper and lower NO asymmetric stretch states and their excitation energies, E_u and E_l, were extracted from the solution of $H(t)$. The distribution of the excitation energies, $\rho(E_{u,l})$, and their mean splitting, ΔE_{sp}, were used as quantitive measures. Throughout the work, we found a classical viewpoint to aid our conclusions in no small measure.

The simplest model for the time-dependent Hamiltonian that we consider comprises only the two NO asymmetric stretch modes perturbed by the solvent forces. The mode pair defines an *xy*-like planar space, and they are also intramolecularly coupled through a cubic anharmonic term of strength *f*. Within this framework, we find that a core sextet of states suffices to capture the solvent effects on the fundamentals. This sextet consists of the ground state, the two fundamentals, and the three first overtones in the two-mode space. Through such a scheme, we find $E_{u,l} \propto \pm fF$. Here, F is the magnitude of the instantaneous, in-plane solvent force, **F**, whose appropriate orthogonal projections, F_x and F_y, are the forces on the NO asymmetric stretches.

A two-mode classical treatment also yields the very same variation for the harmonic frequencies of the two modes. The solvent forces act through the cubic anharmonicity to affect the quadratic potential of the NO asymmetric stretches and hence their frequencies. This is also seen as the root cause of the effect in the above quantum approach. The simulations yield water

solvent forces on the mode pair, F_x and F_y, that have a Gaussian spread with $\sigma(F_{x,y}) \approx 100\ cm^{-1}$. Thereby, F's distribution takes a Maxwell−Boltzmann form and so does $\rho(E_{u,l})$. The mean splitting, $\Delta E_{sp} \propto f\langle F\rangle$, is computed to be 24.4 cm^{-1}.

Upon moving to a full, six-mode treatment that includes solvent forces on all modes, we find that (the six-mode version of) the core sextet still suffices to obtain a converged $\rho(E_{u,l})$. Inclusion of several other states was found to have no significant effect on the distribution or the mean splitting. Dissecting the nature of their couplings to the NO asymmetric stretches, these extra states were seen to either have too weak of a perturbative energy shift effect or (as a group) to simply provide an energy offset.

The six-mode E_u and E_l distributions are, however, broader than the two-mode ones and have a slightly smaller mean splitting. The cause of the latter effect is identified as the in-plane bend forces. Their effect on the E_u and E_l values is similar to that of the NO asymmetric stretch forces, though weaker and in the opposite direction. The final mean splitting obtained in our treatment is 21.7 cm^{-1}. The solvent force on the symmetric stretch adds significantly to the breadth of $\rho(E_{u,l})$ without changing the splitting. The NO symmetric stretch, by its very nature, affects the harmonic frequencies of all of the other modes with a strength depending on the latter's excitation level. In our specific case, it shifts both of the NO asymmetric stretches to a greater extent than the ground state, though synchronously. In both the classical and quantum approaches, this translates to the observed broadening.

Most of the analysis presented in this article neglects the force gradients on the modes. When included in either the two-mode or six-mode time-dependent Hamiltonians, they have only a slight effect on the mean splittings and eigenvalue distributions. The sizes of the force gradients are an order of magnitude smaller than the forces, and their effect is further reduced in some cases by small prefactors arising from weak intramolecular couplings.

A striking feature of the present results is the a priori unexpected validity of the two-mode description of sections 3.2 and 3.3 (and even the classical description of section 3.1) for the nitrate ion in aqueous solution. The much more sophisticated analysis of section 4 hardly changes the splitting predicted by the two-mode treatments and only modestly distorts the eigenvalue distributions. The reasons for this outcome are given in detail in section 4. It is worth pointing out that this simplicity (if maintained with dynamical effects included) provides a useful perspective for thinking about the infrared spectrum and the band splitting.

On the other hand, it is quite possible that other situations for nitrate at higher concentrations with significant ionic effects, including cation influence, and for environmentally important molecular anions, such as SO_4^{2-} [29] and CO_3^{2-},[30] with potentially stronger anion−water interactions[16] would not display the same few-mode simplification. Our sequence of analysis, appropriately adapted, may nonetheless provide a useful approach here.

An interesting aspect of our results is the absence of a noticeable dependence on the in-plane orientation, θ, of the NO asymmetric stretch forces (see eq 8). This angle may be perceived as one of the collective, in-plane markers of the solvent influence. In the two-mode treatment, although θ is formally present in expressions for the excitation energies, its numerical contribution is weak. This is reflected in the invariance of the distributions of these energies with θ (not shown in a figure) as well as the instantaneous and mean splittings. We have numerically checked that these trends for the distributions extend to the six-mode analyses as well, indicating that θ will not have a significant imprint on the observed symmetry breaking. This feature may not persist at high concentrations where ionic effects may have a significant effect on the nitrate charge localization; this might be true of dilute solutions of multiply charged planar anions that exhibit stronger anion−water interaction.[16]

In the present work, we have ignored Coriolis and centrifugal coupling effects. Our estimates[31] of these indicate that they have only a minor effect on the splitting. The lowest order Coriolis couplings increase the eigenvalue splitting by ∼5 cm^{-1}, while the centrifugal couplings (through the second-order expansion term of the inverse moment of inertia) add ∼2 cm^{-1}. These rotational coupling effects will be addressed elsewhere in connection with the spectrum and relaxation dynamics. In particular, the first-order centrifugal coupling may prove important for vibrational energy relaxation via a 2:1 Fermi coupling involving water librations.[32]

In this article, our analyses have been based upon ensemble-averaged quantities, namely, energy distributions and mean splittings. Several dynamical properties remain to be considered, the first of which is the spectrum. Its computation will be an extension of results of this article wherein the time dependence of the NO asymmetric stretch states' descriptions and energies will play a role. Underlying the dynamics of these states are the solvent forces, which, in turn, arise from the relative motion of the nitrate and the neighboring waters. The nature of the relevant solvent motions, local or collective, and the connections to the dynamics of the anion−water and neighboring water−water hydrogen bond motions are interesting avenues that we are presently exploring.

Acknowledgment. This work was supported in part by ANR Grant NT05-4-43154 and by NSF Grant CHE-0750477. S.R. acknowledges the support of a JSPS Postdoctoral Fellowship for Research Abroad. JTH expresses his appreciation of Carl Lineberger as a long-time colleague and friend.

Appendix A. Vibrational Potential Surface

A.1. Choice of Single Reference Geometry. The central premise of this article is that it suffices to treat symmetry breaking in NO_3^- based upon a single, D_{3h}-symmetric reference structure of the anion. One simple support is that the symmetry of the anion's average internal geometry in solution is also D_{3h}. A stronger rationale is that the NO bond length distortions that lead to the observed symmetry breaking are smaller than what the anion already samples in the course of a vibration. We provide some evidence of this claim below.

The mean of the two NO asymmetric stretch band centers is about 1370 cm^{-1}. The experimental splitting of 35−60 cm^{-1},[1,9,11] or individual shifts of about 18−30 cm^{-1} of each mode, is quite small compared to band positions. A slight bond length asymmetry would be sufficient to produce this effect. For instance, Waterland et al. have reported the largest $|\Delta r_{ij}| = |r(NO_i) - r(NO_j)|$ values in optimal (HF/6-311++G**) one- and two-water complexes to be about 0.015 Å, for which the harmonic frequency splittings are ∼40 cm^{-1}. For the three one-water complexes reported in our previous work, $|\Delta r_{ij}|$ are 0.017−0.019 Å (MP2/aug-cc-pVDZ), with the corresponding harmonic splittings in the range of 65−85 cm^{-1}.[16] A complex with one water molecule each on two of the NO_3^- oxygens has $|\Delta r_{ij}| = 0.011$ Å and a harmonic splitting of 80 cm^{-1}. Owing to the small size of these complexes, the cited numbers are likely to be somewhat exaggerated compared to those in aqueous solution but provide a useful reference nonetheless.

TABLE 3: Harmonic Frequencies and Fundamentals, in cm^{-1}, before and after Adjustment

	harm. freqs.		fundamentals		
mode	unadj.	adj.	unadj.	adj.	exp.[a]
1	1066.7	1056.7	1058.8	1046.9	1045
2	830.8	830.8	822.3	821.4	823
3	1486.8	1407.0	1461.0	1376.5	1370
4	706.5	734.0	700.0	726.1	725

[a] These are estimates based on refs 1, 9−11.

We contrast the above Δr_{ij}'s with that for the NO_3^- structure at the turning points of the NO asymmetric stretch vibration. Using the quadratic force constants, we estimate that $|\Delta r_{ij}| = 0.075$ Å for a zero-point vibration, while that for a room-temperature kT vibration is roughly 0.04 Å. Clearly, the bond length changes noted above for the one- and two-water complexes are smaller than even the thermal vibrational amplitude. This is also true of data for several asymmetric 1−8 water structures from Wang et al.,[33] Ebner et al.,[34] as well as our own computations. The optimal Δr_{ij} are typically less than 0.02 Å, with some exceptions in the 0.03−0.035 Å range.

A. 2. Computation of the ω's and Taylor-Expanded V_{anh}. It is convenient to use internal coordinates to define vibrational potentials. Here, we use symmetrized combinations of bond length extension (Δr_i) and angle changes ($\Delta\phi_{ij}$), namely

$$\begin{aligned} S_1 &= \frac{1}{\sqrt{3}}(\Delta r_1 + \Delta r_2 + \Delta r_3) \\ S_2 &= \pm\frac{1}{3^{1/4}}\sqrt{-\Delta\phi_{12} - \Delta\phi_{13} - \Delta\phi_{23}} \\ S_{3x} &= \frac{2}{\sqrt{6}}(-\Delta r_1 - \Delta r_2 + 2\Delta r_3) \\ S_{4x} &= \frac{2}{\sqrt{6}}(-\Delta\phi_{23} - \Delta\phi_{13} + 2\Delta\phi_{12}) \\ S_{3y} &= \frac{1}{\sqrt{6}}(\Delta r_1 - \Delta r_2) \\ S_{4y} &= \frac{1}{\sqrt{6}}(\Delta\phi_{23} - \Delta\phi_{13}) \end{aligned} \tag{30}$$

The numbering and description of these symmetry coordinates match those in Table 1. (The subscripts for the Δr's and $\Delta\phi$'s are oxygen atom labels.) The form of S_2, the out-of-plane bend, was taken from Pesonen et al., who employed it as a robust coordinate for the NH_3 inversion problem.[35] Its sign, $\mathbf{r}_1 \cdot \mathbf{r}_2 \times \mathbf{r}_3/|\mathbf{r}_1 \cdot \mathbf{r}_2 \times \mathbf{r}_3|$, signals whether the N atom is above or below the oxygen plane.

A full quartic Taylor expansion was developed in **S**. For this, ab initio computations at the MP2/aug-cc-pVDZ level were carried out using Gaussian 03.[36] The optimal equilibrium bond length at this theory level is 1.2687 Å. Distorted nitrate geometries were generated by displacement along one ($S_i = n\delta$) or two ($S_i = n\delta$, $S_j = m\delta$, $i \neq j$) coordinates. For each structure, Cartesian first and second potential derivatives are extracted and transformed to symmetry coordinate derivatives as follows

$$\frac{\partial^2 V(\mathbf{S})}{\partial S_i \partial S_j} = \frac{\partial \mathbf{x}_k(\mathbf{S})}{\partial S_i} \cdot \frac{\partial^2 V(\mathbf{S})}{\partial \mathbf{x}_k \partial \mathbf{x}_l} \cdot \frac{\partial \mathbf{x}_l(\mathbf{S})}{\partial S_j} + \frac{\partial V(\mathbf{S})}{\partial \mathbf{x}_k} \cdot \frac{\partial^2 \mathbf{x}_k(\mathbf{S})}{\partial S_i \partial S_j} \tag{31}$$

This is a generally valid equation that accounts for the nonlinear relation between the Cartesian and the symmetry coordinates. Of course, the bracketed **S**'s in the numerators describe the geometry at which the derivatives are evaluated. For $\mathbf{S} = \mathbf{0}$, we obtain the quadratic force field. Numerical differentiations of these transformed derivatives at $\mathbf{S} \neq \mathbf{0}$ yield the third- and fourth-order potential terms. A uniform step size of 0.02 units for all six S_i's was found to give converged derivatives with a five-point numerical difference formula. The symmetry within each expansion order was verified and coefficients of related terms averaged to eliminate any small numerical differences. As such, given a random distorted NO_3^- structure with an ab initio energy under 5000 cm^{-1} (relative to the potential minimum), this quartic potential has an absolute error of ~8 cm^{-1}. The discrepancy increases to ~35 cm^{-1} for the 5000−10000 cm^{-1} range.

At each geometry used above, we also automatically obtain the ab initio dipole moment, its derivatives in Cartesian space, as well as the polarizability tensor. These can be numerically differentiated as well to obtain the dipole moment surface and polarizability surface up to second order for future use in the spectrum calculations.

Before we proceed, we take cognizance of two practical issues. First, only aqueous-phase frequencies are available for nitrate; therefore, the above ab initio potential $V(\mathbf{S})$ cannot be independently tested. Second, it would be rather fortuitous for a solute−solvent interaction, when ensemble-averaged and added to an appropriate vacuum potential, to yield near-correct gas-to-solution-phase frequencies shifts. Given the need for reasonably well-positioned states suited to the aqueous-phase problem, we employ the common, minimalistic procedure of adjusting the diagonal terms of the quadratic portion of $V(\mathbf{S})$. The harmonic frequencies are thereby altered, and Table 3 summarizes the changes affected. We show the expansion of $V(\mathbf{S})$ in Table 4.

In order to facilitate the computation of eigenstates, we switch to rectilinear normal coordinates in their unitless form, **Q**. (The regular form is given as $q_i = (\hbar/\omega_i)^{1/2}Q_i$.) Their main advantage is the uncomplicated kinetic energy operator, $\hat{K} = -\sum_i (1/2)\omega_i(\partial^2/\partial Q_i^2)$, assuming negligible vibrational angular momentum. Computing $V(\mathbf{Q})$ is straightforwardly done via a fifth-order expansion of **S** in terms of **Q**. With the minimum order of $V(\mathbf{S})$ being 2, this generates a sixth-order normal coordinate potential, $\sum_i (1/2)\omega_i Q_i^2 + V_{anh}$ of eq 1.

Appendix B. Simulation Details

The nitrate−water system has been simulated using the standard NVE molecular dynamics protocols. We use an interaction potential (set B) constructed by Thomas et al.,[18] which defines polarization parameters for nitrate and uses POL3 as the water model. The setup consists of a single NO_3^- ion in a cubic box of 255 water molecules, with no counterion included. The box size is computed assuming pure water solution density (0.997 g/cm^3). We have used the shifted-force form of the Lennard-Jones interaction and the Ewald summation method for long-range electrostatics.[37] For the induced atomic dipoles, the convergence threshold was set to 10^{-6} Debye.

All species in the box were held rigid during the simulations; the internal structure of NO_3^- was that employed in building the reference Hamiltonian (Appendix A.2). Using a time step of 0.5 fs, several production runs of 250 ps length were executed. The trajectory was written out every 4 fs. The force gradients on the anion atoms were numerically computed at the same frequency and saved along with the forces.

TABLE 4: Symmetry Coordinate Potential for Isolated NO_3^- [a]

5.26161	S_1^2	1.18260	S_2^2	3.37284	S_{3x}^2,S_{3y}^2	0.89537	S_{4x}^2,S_{4y}^2	−0.77559	$S_{3x}S_{4x},S_{3y}S_{4y}$
−7.14223	S_1^3	1.05412	$S_{3x}S_{3y}S_{4y}$	−1.31538	$S_2^2S_{3x}S_{4x}$	8.38301	$S_{3x}^2S_{3y}^2$	1.53623	$S_1^2S_{4y}^2$
−2.35832	$S_1S_2^2$	−1.20529	$S_{4x}S_{3y}S_{4y}$	2.11783	$S_1S_{3x}^2S_{4x}$	−2.11783	$S_1S_{4x}S_{3y}^2$	0.98347	$S_2^2S_{4y}^2$
−15.59518	$S_1S_{3x}^2$	−1.42644	$S_1S_{4y}^2$	−0.12548	$S_{3x}^3S_{4x}$	−0.12548	$S_{3x}S_{4x}S_{3y}^2$	1.25771	$S_1S_{3x}S_{4y}^2$
−3.62179	S_{3x}^3	−0.60265	$S_{3x}S_{4y}^2$	1.53623	$S_1^2S_{4x}^2$	−0.01845	$S_{4x}^2S_{3y}^2$	−0.01845	$S_{3x}^2S_{4y}^2$
2.27464	$S_1S_{3x}S_{4x}$	0.63071	$S_{4x}S_{4y}^2$	0.98347	$S_2^2S_{4x}^2$	4.19151	S_{3y}^4	−1.26642	$S_1S_{4x}S_{4y}^2$
−0.52706	$S_{3x}^2S_{4x}$	7.60674	S_1^4	−1.25771	$S_1S_{3x}S_{4x}^2$	−3.20876	$S_1^2S_{3y}S_{4y}$	−0.51484	$S_{3x}S_{4x}S_{4y}^2$
−1.42644	$S_1S_{4x}^2$	2.32547	$S_1^2S_2^2$	0.64085	$S_{3x}^2S_{4x}^2$	−1.31538	$S_2^2S_{3y}S_{4y}$	0.41681	$S_{4x}^2S_{4y}^2$
0.60265	$S_{3x}S_{4x}^2$	0.67221	S_2^4	0.42214	$S_1S_{4x}^3$	−4.23567	$S_1S_{3x}S_{3y}S_{4y}$	0.64085	$S_{3y}^2S_{4y}^2$
−0.21024	S_{4x}^3	37.16155	$S_1^2S_{3x}^2$	−0.51484	$S_{3x}S_{4x}^3$	−0.12548	$S_{3x}^2S_{3y}S_{4y}$	−0.51484	$S_{3y}S_{4y}^3$
−15.59518	$S_1S_{3y}^2$	0.76278	$S_2^2S_{3x}^2$	0.20841	S_{4x}^4	2.51542	$S_1S_{4x}S_{3y}S_{4y}$	0.20841	S_{4y}^4
10.86536	$S_{3x}S_{3y}^2$	12.96590	$S_1S_{3x}^3$	37.16155	$S_1^2S_{3y}^2$	1.31860	$S_{3x}S_{4x}S_{3y}S_{4y}$		
0.52706	$S_{4x}S_{3y}^2$	4.19151	S_{3x}^4	0.76278	$S_2^2S_{3y}^2$	−0.51484	$S_{4x}^2S_{3y}S_{4y}$		
2.27464	$S_1S_{3y}S_{4y}$	−3.20876	$S_1^2S_{3x}S_{4x}$	−38.89769	$S_1S_{3x}S_{3y}^2$	−0.12548	$S_{3y}^3S_{4y}$		

[a] The expansion has the form $\sum_{i\le j} f_{ij}S_iS_j + \sum_{i\le j\le k} f_{ijk}S_iS_jS_k + \sum_{i\le j\le k\le l} f_{ijkl}S_iS_jS_kS_l$ with all factorials absorbed into the unique coefficients. The potential constants are in aJ/Å^n, (a = atto) where n is the number of nonangular symmetry coordinates in a given term. The quadratic terms (first line) have been adjusted (see Appendix A.2), while the cubic and quartic terms are directly from ab initio calculations.

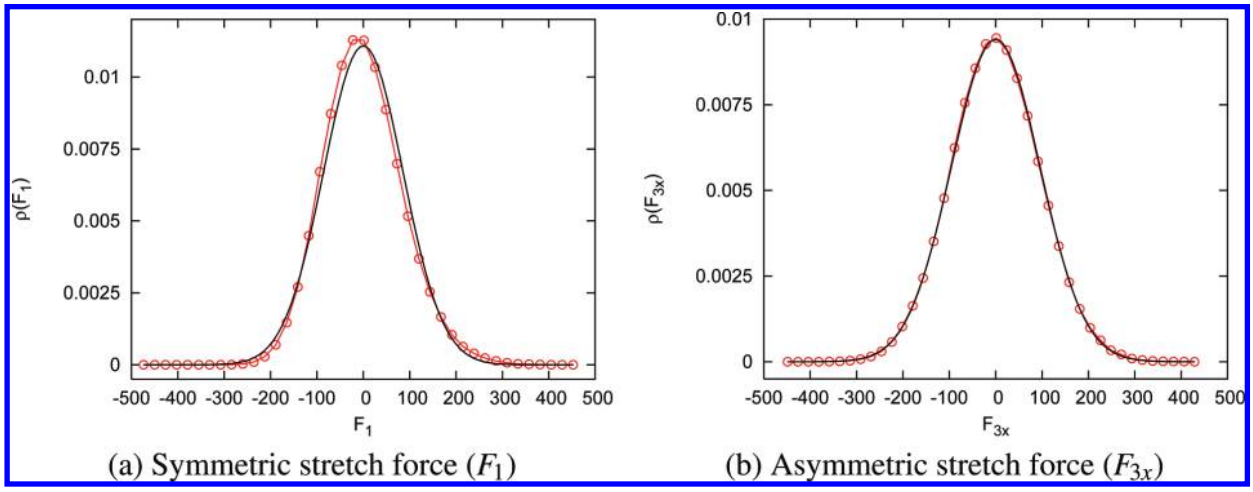

Figure 7. Comparison of the distribution of forces from the simulation and a Gaussian fit to them. Shown are the plots for the symmetric and asymmetric stretches. See the text in Appendix B for details.

Postsimulation processing involved extracting the solute−solvent interaction potential, $\delta V(t)$, from these saved Cartesian forces and force gradients. They were first rotated to the body frame of the anion and then linearly transformed into unitless rectilinear normal coordinates, **Q**. The averages of these quantities over the trajectory length were subtracted since we needed only the fluctuating part of the solvent influence on the anion's modes, that is, eq 2.

The final forces, F_i, and force gradients, G_{ij}, were found to have Gaussian distributions. The σ values of the normalized distributions for the forces on modes 1−4 are about 86, 180, 95, and 117 cm^{-1}, respectively. A comparison of the distribution shapes having these widths and the simulation data is provided in Figure 7. Evidently, F_1's from the simulation have a slightly lopsided spread. Since the associated coordinate, Q_1, is a key coordinate, this feature will be worth analysis, a task we leave for the future. The other five mode forces, however, straightforwardly follow a Gaussian distribution, as exemplified by the plot for F_{3x}. This greatly simplifies analyses of distributions of quantities based upon these forces; particularly, those for F_{3x} and F_{3y} are directly used in section 3.

The σ's for the G_{ij} are in the 1−10 cm^{-1} range. Among the forces, only pairs (F_{3x},F_{4x}) and (F_{3y},F_{4y}) have a nonzero normalized covariance of 0.475 each. Several $F-G$ and $G-G$ pairs of the same symmetry also exhibit non-negligible covariance.

Appendix C. Explanation of the Weak Effect of the Extra-Sextet States

In this Appendix, we consider the states that could potentially produce a sizable solvent-induced influence on the ν_3 energy splitting and distribution. The list comprises states with 1 or 2 quanta of excitation in their leading basis functions.

The first ones that we target are the in-plane bend overtones, $2\nu_4$ (A_1, E_x, E_y), which lie only ∼75 cm^{-1} above the ν_3 fundamentals. The leading basis functions of ν_{3x} and ν_{3y} are 3_1^x, 3_1^y, $1_13_1^x$, and $1_13_1^y$. The first two cannot couple, through the linear terms in $\delta V(t)$, to an important expansion term for any of the three bend overtones; see Table 2. The latter two do have coupling partners (e.g., 3_1^x in $2\nu_{4x}$, 3_1^y in $2\nu_{4y}$, and 1_1 in $2\nu_{4A}$). The magnitudes of these interactions are estimated to be typically under 1 cm^{-1}, which, in themselves, cause a negligible perturbative $\nu_{3x(y)}$ energy shift. Scanning through all five eigenfunction expansions in this manner, we estimate that the combined solvent-induced coupling magnitude for each bend overtone−stretch fundamental pair is roughly 1−2 cm^{-1} and thus small enough compared to the energy separation to be ineffectual on the ν_3 energies. The above statements assume the dynamical gap between the state sets to be at least a few 10's of wavenumbers. Support for this comes from our simulation result that the time-varying energy gap between the

upper ν_3 state and lowest bend overtone is rarely and briefly below 20 cm^{-1}.

We now examine the role of states $\nu_2 + \nu_{3x}$ and $\nu_2 + \nu_{3y}$. Through $-F_2Q_2$, the two couple to ν_{3x} and ν_{3y}, respectively. Through the same solvent force term, ν_2 couples to the ground state as well. These couplings are largely $-F_2\langle a_m|Q_2|2_1a_m\rangle$, $a_m = 0_0,3_1^x,3_1^y$. All three have the same value of $-F_2/2^{1/2}$. In perturbation theory language, this means that ν_2 pushes the ground state down by $F_2^2/2\omega_2$, which is just as much as the $\nu_{3x(y)}$ push-down due to $\nu_2 + \nu_{3x(y)}$. Clearly, the trio examined here does not cause any net effect to the ν_3 excitation energies. The magnitude of the shift betrays the root cause of the lack of change, namely a shift in the potential minimum for Q_2. The harmonic potential for Q_2 with the solvent force is rewritten as follows

$$\frac{1}{2}\omega_2 Q_2^2 - F_2Q_2 = \frac{1}{2}\omega_2\left(Q_2 - \frac{F_2}{\omega_2}\right)^2 - \frac{F_2^2}{2\omega_2}$$

The couplings appear in the quantum treatment due to the use of functions and states centered at the reference geometry rather than the shifted one. We chose Q_2-related states in this paragraph solely for the ease of arguments with them. The reader will easily see that the same applies to the ν_{4x}, ν_{4y}, and the four $\nu_3 + \nu_4$ combinations, as well as to ν_1 and $\nu_1 + \nu_{3x(y)}$.

It remains for us to address the coupling $\nu_{3x(y)}$ to all of the other fundamentals as well as a few overtones that do not involve ν_3. In principle, these could add to the ν_3 splitting and/or give the pair an extra energy shift relative to the ground state (leading to a wider distribution). We quickly find that ν_2, $\nu_{4x(y)}$, their overtones, their 1:1 combination with ν_1, as well as $\nu_2 + \nu_{4x(y)}$ (most of these are not shown in Table 2) have a weak perturbative influence on the ν_3 energies. For ν_1 and $2\nu_1$, however, a more careful look is warranted. Apropos the former, note that its leading function, 1_1, can couple to $1_13_1^{x(y)}$, which are the second most important terms of the $\nu_{3x(y)}$ expansions, with a coefficient as high as 0.2. We estimate $|\langle\nu_1|\delta V(t)|\nu_{3x(y)}\rangle|$ to be in the $10-20$ cm^{-1} range. This is a largish value, though not large enough to prevail over the $\sim$330 cm^{-1} energy gap denominator. The resulting upward energy shifts of ν_{3x} and ν_{3y} are expected to be both under $1-2$ cm^{-1} but different in value. These sizes are not insignificant yet are apparently subdued in Figure 5. This could be due to partial cancellation with the effect of $2\nu_1$. This overtone's expansion (not shown) contains $0.32\cdot(1/2^{1/2})(3_1^x4_1^x + 3_1^y4_1^y)$. The resulting coupling size is expected to be $15-20$ cm^{-1}. With a $\nu_3 - 2\nu_1$ energy gap of $\sim$700 cm^{-1}, a downward shift of $0.5-1$ cm^{-1} may be estimated.

References and Notes

(1) (a) Gibson, E. R.; Hudson, P. K.; Grassian, V. H. *J. Phys. Chem. A* **2006**, *110*, 11785–11799. (b) Hudson, P. K.; Schwarz, J.; Baltursaitis, J.; Gibson, E. R.; Grassian, V. H. *J. Phys. Chem. A* **2007**, *111*, 544–548.

(2) Solomon, S. *Rev. Geophys.* **1999**, *37*, 275–316.

(3) (a) Guimbaud, C.; Arens, F.; Gutzwiller, L.; Gäggeler, H. W.; Ammann, M. *Atmos. Chem. Phys. Discuss.* **2002**, *2*, 739–763. (b) Davies, J. A.; Cox, R. A. *J. Phys. Chem. A* **1998**, *102*, 7631–7642. (c) Beichert, P.; Finlayson-Pitts, B. J. *J. Phys. Chem. A* **1996**, *100*, 15218–15228. (d) Ghosal, S.; Hemminger, H. C. *J. Phys. Chem. B* **2004**, *108*, 14102–14108.

(4) (a) Rivera-Figueroa, A. M.; Sumner, A. L.; Finlayson-Pitts, B. J. *Environ. Sci. Technol.* **2003**, *37*, 548. (b) Mochida, M.; Finlayson-Pitts, B. J. *J. Phys. Chem. A* **2000**, *104*, 9705–9711. (c) Saliba, N. A.; Yang, H.; Finlayson-Pitts, B. J. *J. Phys. Chem. A* **2001**, *105*, 10339–10346.

(5) Abbatt, J. P. D. *Geophys. Res. Lett.* **1997**, *24*, 1497.

(6) (a) Wang, S.; Bianco, R.; Hynes, J. T. *J. Phys. Chem. A* **2009**, *113*, 1295–1307. (b) Bianco, R.; Wang, S.; Hynes, J. T. *J. Phys. Chem. A* **2008**, *112*, 9467–9476. (c) Bianco, R.; Wang, S.; Hynes, J. T. *J. Phys. Chem. A* **2007**, *111*, 11033–11042. (d) Shamay, E. S.; Buch, V.; Parrinello, M.; Richmond, G. L. *J. Am. Chem. Soc.* **2007**, *129*, 12910–12911. (e) Ardura, D.; Donaldson, D. J. *Phys. Chem. Chem. Phys.* **2009**, *11*, 857–863.

(7) (a) Schnitzer, C.; Baldelli, S.; Shultz, M. J. *J. Phys. Chem. B* **2000**, *104*, 585–590. (b) Kido Soule, M. C.; Blower, P. G.; Richmond, G. L. *J. Phys. Chem. A* **2007**, *111*, 3349–3357.

(8) (a) Waterland, M. R.; Kelley, A. M. *J. Chem. Phys.* **2000**, *113*, 6760–6773. (b) Waterland, M. R.; Stockwell, D.; Kelley, A. M. *J. Chem. Phys.* **2001**, *114*, 6249–6258.

(9) (a) Irish, D. E.; Walrafen, G. E. *J. Chem. Phys.* **1967**, *46*, 378–384. (b) Irish, D. E.; Davis, A. R. *Can. J. Chem.* **1968**, *46*, 943–951. (c) Irish, D. E.; Davis, A. R.; Plane, R. A. *J. Chem. Phys.* **1969**, *50*, 2262–2263. (d) Davis, A. R.; Macklin, J. W.; Plane, R. A. *J. Chem. Phys.* **1969**, *50*, 1478–1479. (e) Chang, T. G.; Irish, D. E. *J. Phys. Chem.* **1973**, *77*, 52–57. (f) Peleg, M. *J. Phys. Chem.* **1972**, *76*, 1019–1025. (g) Findlay, T. J.; Symons, M. C. *J. Chem. Soc., Faraday Trans. 2* **1976**, *72*, 820–826.

(10) Zhang, Y.-H.; Choi, M. Y.; Chan, C. K. *J. Phys. Chem. A* **2004**, *108*, 1712–1718.

(11) Liu, J.-H.; Zhang, Y.-H.; Wang, L.-Y.; Wei, Z.-F. *Spectrochim. Acta, Part A* **2005**, *61*, 893–899.

(12) While this ν_3 doublet is perhaps the most easily noted spectral feature, other bands of NO_3^- also reflect the lowered symmetry in solution. The ONO in-plane bend mode pair, degenerate in vacuum, also splits in solution (ν_4, $\sim$725 cm^{-1}), though only noted at high concentrations. The symmetric stretch (ν_1, $\sim$1045 cm^{-1}) is IR-disallowed for the isolated anion but is visible in aqueous solution.

(13) Lebrero, M. C. G.; Bikiel, D. E.; Elola, M. D.; Estrin, D. A.; Roitberg, A. D. *J. Chem. Phys.* **2002**, *117*, 2718–2725.

(14) Boisson, J. Ph.D. Thesis, UPMC (Paris 6) and ENS-Paris, 2008.

(15) Boisson, J.; Laage, D.; Hynes, J. T. In preparation.

(16) Ramesh, S. G.; Re, S.; Hynes, J. T. *J. Phys. Chem. A* **2007**, *112*, 3391–3398.

(17) It has been shown previously that the constant part of these average force gradients could result in blue shifting relative to the vacuum: Rey, R.; Hynes, J. T. *J. Chem. Phys.* **1998**, *108*, 142–153.

(18) Thomas, J. L.; Roeselová, M.; Dang, L. X.; Tobias, D. J. *J. Phys. Chem. A* **2007**, *111*, 3091–3098. The reference, and articles cited therein, may be consulted for work on the issue of NO_3^-'s preference (or lack thereof) for an aqueous surface location.

(19) (a) Oxtoby, D. W.; Levesque, D.; Weis, J. J. *J. Chem. Phys.* **1978**, *68*, 5528. (b) Rey, R.; Hynes, J. T. *J. Chem. Phys.* **1996**, *104*, 2356–2368. (c) Rey, R.; Moller, K. B.; Hynes, J. T. *J. Phys. Chem. A* **2002**, *106*, 11993–11996. (d) Lawrence, C. P.; Skinner, J. L. *Chem. Phys. Lett.* **2003**, *369*, 472–477. (e) Li, S.; Shepard, T. D.; Thompson, W. H. *J. Phys. Chem. A* **2004**, *108*, 7347–7355.

(20) We point out that the force gradients can themselves lead to a nonzero splitting, even if the F's were turned off by setting $\alpha = 0$. The splitting in such a case is about 4.1 cm^{-1}.

(21) Had the eigenfunctions of the two fundamentals contained a $v = 3$ function, each with a coefficient of c_3, their contribution to the diagonal block would have been proportional to $c_2c_3F_{x(y)}$. However, since $|c_3| < |c_2|$ and c_2 is already small (see eq 13), these additions can be ignored.

(22) Note that the splitting values in all cases are a bit larger than the gap between the peak positions of $\sim$22 cm^{-1}, owing to the Maxwell–Boltzmann shape of the distribution.

(23) Apropos the basis set, we actually use a "polar" version that is related to the traditional set by a complex linear transformation. This alternate basis is well suited for the treatment of degenerate vibrations and renders the identification and application of symmetry properties very simple; see: Cohen-Tannoudji, C.; Diu, B.; Laloë, F. *Quantum Mechanics*; Wiley: New York, 1977; Vol. 1. In particular, each polar basis function is either already of a defined symmetry type or requires only a pair combination. Once the eigenstates are computed in this basis, we switch back to the traditional basis at a suitable stage.

(24) We remark parenthetically that while these two states do not strongly affect each others' energies, the mixing is nevertheless important in the context of energy flow. With no other intramolecular states in the vicinity, it could well be that ν_3 excitation decay to the water solvent is via the $2\nu_4$ states as the doorway.

(25) Note, however, that the 2m reference eigenvalues, $E_{o,l}^{2m}$, that occur along the diagonal in eq 15 will be replaced by their all-mode values. The latter are given in Table 2.

(26) This frequency shift is incorrect for Q_1 itself. The appropriate treatment may be found, for instance, in: Goldstein, H. *Classical Mechanics*, 2nd ed.; Addison-Wesley: Reading, MA, 1980. However, we do not need such refinement to make our case presently.

(27) The cubic terms that we have considered here are formally no different from that in the previous section on the in-plane bends (few lines

below eq 25). However, we saw no ground-state effect there. At a classical level, this is because the mode 3 harmonic frequencies are split, $\omega_3' \approx \omega_3 \pm c_1|c_b|F_4$, $F_4 = (F_{4x}^2 + F_{4y}^2)^{1/2}$. This shows that neither is the energy of the harmonic ground state shifted due to a cubic term nor is the midpoint of the two fundamental energies. Regarding Q_2, the anharmonic term $Q_2(Q_{3x}^2 + Q_{3y}^2)$ is symmetry-disallowed.

(28) These are identified as the states that overlap best with "pure" ν_3 vectors, the latter being provided by a second diagonalization of $H(t)$ with the core sextet as the basis. We had no numerical difficulty in implementing this scheme, and the average of the squared overlap was found to be 0.94. This high value tells us that, though there is some important state mixing caused by the solvent, the matched states are still predominantly ν_3 in character.

(29) (a) Rudolph, W. W.; Brooker, M. H.; Tremaine, P. *Z. Phys. Chem.* **1999**, *209*, 181–207. (b) Zhou, J.; Santambrogio, G.; Brümmer, M.; Moore, D. T.; Wöste, L.; Meijer, G.; Neumark, D. M.; Asmis, K. R. *J. Chem. Phys.* **2006**, *125*, 111102. (c) Bush, M. F.; Saykally, R. J.; Williams, E. R. *J. Am. Chem. Soc.* **2007**, *129*, 2220–2221. (d) Saito, Y.; Hamaguchi, H. *Chem. Phys. Lett.* **2001**, *339*, 351–356.

(30) Rudolph, W. W.; Fischer, D.; Irmer, G. *Appl. Spectrosc.* **2006**, *60*, 130–144.

(31) Ramesh, S. G.; Re, S.; Boisson J.; Hynes, J. T. Unpublished.

(32) (a) Ingrosso, F.; Rey, R.; Elsaesser, T.; Hynes, J. T. *J. Phys. Chem. A* **2009**, *113*, 6657–6665. (b) Rey, R.; Ingrosso, F.; Elsaesser, T.; Hynes, J. T. *J. Phys. Chem. A* **2009**, *113*, 8949−8962.

(33) Wang, X.-B.; Yang, X.; Wang, L.-S.; Nicholas, J. B. *J. Chem. Phys.* **2002**, *116*, 561–570.

(34) Ebner, C.; Sansone, R.; Probst, M. *Int. J. Quantum Chem.* **1998**, *70*, 877–886.

(35) Pesonen, J.; Miani, A.; Halonen, L. *J. Chem. Phys.* **2001**, *115*, 1243–1450.

(36) Frisch, M. J.; et al. *Gaussian 03*, revision C.02; Gaussian, Inc.: Wallingford, CT, 2004.

(37) Frenkel, D.; Smit, B. *Understanding molecular simulation: From algorithms to applications*; Academic Press: San Diego, CA, 2002.

JP903626T